Mechanics and Control of Coupled Interactions in Ambient Media

Blake Rhyan Buchanan
CMU-RI-TR-20-43
July 1, 2020

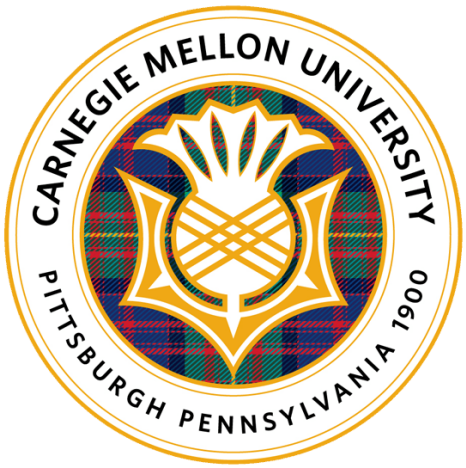

The Robotics Institute
School of Computer Science
Carnegie Mellon University
Pittsburgh, PA

Thesis Committee:
Professor Matthew Travers
Professor Howie Choset
Professor Scott David Kelly
Jaskaran Singh Grover

Submitted in partial fulfillment of the requirements
for the degree of
Master of Science in Robotics

Abstract

Many multi-agent systems in nature comprise agents that interact with, and respond to, the dynamics of their environment. For example, fish school based on the fundamental fluid phenomena of vortex shedding, birds shed leading-edge vortices in formation for flocking, and *E. coli* bacteria secrete and push against a surrounding medium to meander in swarms. In this thesis, we investigate the mechanics and control of three different systems having agents that interact with a surrounding medium to affect motion. We make use of the *Chaplygin beanie*, a planar underactuated nonholonomic mechanical system outfitted with a rotor atop its body and a single wheel at its rear constraining its dynamics to the plane about which it moves. We first consider a single passively compliant Chaplygin beanie atop a platform having translational compliance, introduce the reduced equations for the system using the notion of symmetry and nonholonomic momentum, and provide proof for a particular stable behavior under arbitrary deformations of the elastic element modeling its compliance. We then direct our focus to results concerning the frequency response and control of passive Chaplygin beanies under actuation of the platform, discuss rich dynamical features arising from periodic actuation, and develop rules by which control can be exerted to collect and disperse multiple such passive vehicles. We then discuss how the latter of these results clarifies the extent to which stable behavior can be excited in the system through exogenous control.

We then leverage our understanding of the single Chaplygin beanie model to inform a geometric treatment of two such agents atop a compliant platform, again invoking symmetry and nonholonomic reduction for analysis. We discuss stability, control, and an entrainment phenomena within this multi-agent dynamical system, present results in the form of simulation, and draw analogies between its behavior and related behaviors within biological systems.

Finally, we introduce the dynamic model for a novel fluid-propulsive aquatic vehicle in an ideal fluid that exerts control over its motion using impulsive fluid-ejection events to move in its environment. We present an analysis concerning the entrainment of a cylindrical-shaped aquatic agent in flows induced by neighboring agents, present preliminary results of an agent position-stabilizing at a desired setpoint using impulsive fluid-ejection events, and discuss the next steps necessary to model multiple such agents in an inviscid fluid.

Acknowledgements

First and foremost, I want to thank my advisors, Professors Matthew Travers and Howie Choset, for the opportunity to explore such an interesting and unique field of work. Your motivation and support of my explorations of mechanics, geometry, control, and communication, is indeed unprecedented. Not many robotics students have the privilege to investigate the fundamental problems we have pursued and I am grateful for what we have begun to uncover. In the same light, I want to extend my deepest thanks to Professor Scott D. Kelly. The content of this thesis is largely attributed to the inspiration you instilled for the beauty underlying geometry, mechanics, and their role in robotics. The countless discussions on these topics and the toy problems motivating them are invaluable and have made a lasting impression. Additionally, I thank Peggy and B.J. for the entirety of their support within the Biorobotics lab and Robotics Institute, respectively. I also want to thank my friends and family for all of the support they provided over the years as I remained engaged in my studies up to this point. Finally, I thank Saumya Saxena, whose love and support have on countless occasions proven critical in the successful generation of this thesis.

Contents

List of Tables

List of Figures

Chapter 1

Introduction

1.1 Overview

In multi-agent robotic systems, it is not often that we consider the different and rich ways in which agents interact in their environment, especially when that environment possesses complicated dynamics of its own. In nature, however, there exist an abundance of systems which contain agents that move about in environments that respond dynamically to the locomotion of neighboring agents. Fish schools, bacterial swarms, and migratory cell groups are but a few, impacting their environment, say by shedding vortices in a fluid or pushing against surrounding compliant substrates, to affect motion. This particular class of systems exhibits the property that agent dynamics are *coupled* through such substrates, motivating a deeper understanding of the mechanics underlying multi-agent coordination when considering the impact of substrate dynamics on agents. In this thesis, we study three example systems, two of which differ only in the number of agents present in the environment. As we will see later, this simple difference in the number of agents drastically increases the complexity of its dynamics.

The first two of these systems are rooted in nonholonomic mechanics, dating back to work by Sergey Chaplygin [1] in which he introduced the simple mechanical system of a sleigh with frictionless casters at its front and constrained at a particular point on its body by what he called a knife-edge. This "knife-edge" effectively permits translational motion in a particular direction relative to a body-fixed frame, but allows no motion in the direction lateral to the translational direction at the contact point of the knife-edge. Mechanical systems constrained in this way are often suitable for modeling biological organisms and their locomotion, e.g., snakes and fish, and have recently shown promise in problems involving multi-agent coordination and control [2]. Much like Chaplygin's sleigh, the system we use in our analysis is effectively a Chaplygin sleigh, but with a symmetric rotor fixed atop its body, called the Chaplygin beanie. Variations in the rotor's angle with respect to time induces locomotion. In this thesis, we equip the Chaplygin beanie with a linear torsional spring, coupling its body to its rotor so that deformations in the rotor relative to the body give rise to passive dynamics and therefore locomotion. Furthermore, we place the Chaplygin atop a platform with finite inertia capable of translational motion, effectively modeling a medium with which the agent can interact. We use nonholonomic reduction to obtain a reduced representation of the dynamics of this system and prove that, given arbitrary deformations in the linear torsional spring, the Chaplygin beanie will asymptotically locomote stably in the forward translational direction. We then present a special case of this problem for which we assume direct control over the platform so as to induce locomotive behaviors of Chaplygin beanies, termed *exogenous control*. The second of these systems is that of *two* Chaplygin beanies atop a platform with translational compliance.

We again invoke nonholonomic reduction via symmetries to obtain a reduced representation of the dynamics and motivate its use in proving asymptotic behaviors.

Finally, we study a cylindrical-shaped agent in an inviscid flow with point vortices. This system is distinct from the previous two in that the medium with which agents interact no longer *directly* couples the motions between agents and their environment. We develop the dynamics for the system, investigate an entrainment phenomenon, and present preliminary results of PID control of the system through impulsive fluid-ejection events.

1.2 Prior Work

Nonholonomic mechanics and locomotion. The general analysis of mechanical systems through the lens of geometry was discussed at length by Marsden [3, 4, 5] and Bloch [6]. We draw inspiration from these works in our analysis of the systems of interest in this thesis. In particular, mechanical systems exhibiting nonholonomic constraints have recently been of utility in studying the effects of compliance in biological agents as well as the role of media coupling the dynamics of such agents. For example, systems like the *Chaplygin beanie* [7], *snakeboard* [8, 9], landfish [10], and various *nonholonomic snake robots* [11, 12], have proven to be motivating examples in the control of biologically inspired robots. Specifically, the passive response many biological agents exhibit due to the natural compliance of joints or connective tissues has inspired the use of torsional springs to model compliance in mechanical systems with nonholonomic constraints [13]. The utility in using reduced representations for proving the stability of such nonholonomic systems was demonstrated in [7] and [10]. Additionally, recent works in multi-agent systems which are coupled to their environment have incorporated such compliant models [2]. This coupling is seen predominantly in natural systems, e.g., schooling fish, swarming bacteria, or migrating cells [14, 15, 16], however, we provide evidence that an understanding of this coupling can be exploited to achieve meaningful behaviors for robotic systems as well. The application of geometric methods to locomotion has also proven useful in the analysis of various other robotic systems including the three-link swimmer [17] and many other biologically inspired systems [18, 19, 20, 21, 22]. Most of these works focus on the agent's locomotion through its environment, but make a reasonable choice to neglect the behavior of the ambient media itself.

The problem of exogenous control has been investigated in the context of transporting particles within a fluid at low Reynolds number using oscillating probes in [23]. Relatedly, [24] used an oscillating probe to excite a substrate containing cardiac cells and showed that the induced deformations of the substrate due to exogenous forcing led to long-term oscillatory behavior in neighboring cardiac cells. A motion planning framework for robotic systems having external configurations, like those moving in dynamic environments, was established in [25].

Locomotion in fluids. A variety of articulated swimming systems have been studied from the perspective of geometric mechanics [26] as well as from a numerical perspective [27, 28, 29]. In this thesis, we study a free cylinder in the presence of point vortices, providing a rich environment for studying agent interactions with an ambient medium. This seemingly simple system has a broad history in the mechanics and controls community. From Kirchhoff's studies in [30] dating back to 1877, Tarleton's in 1892 [31], and Föppl's in 1913 (insert reference), to more recent works like [32], [33], [34], [35], [36], and [37], problems involving rigid bodies interacting with distributions of point vortices remain of significant interest. [32] elucidated the linear and nonlinear stability of the moving circular cylinder in the so-called *moving* Föppl equilibrium. [35] takes a control-theoretic approach for the system by studying the cases of a

circular cylinder with $N = 1$ and $N = 2$ point vortices in the flow, and showing time-optimal controllability for a bounded force acting through the center of mass of the cylinder for the $N = 1$ case. [37] develops the equations of motion for a circular cylinder in the presence of N point vortices from a geometric perspective and shows that the resulting equations of motion obtained in [32] and [34] are equivalent.

Chapter 2

Background

2.1 Mathematical Preliminaries

In the chapters that follow, we will utilize various mathematical tools and ideas in order to properly describe the dynamical systems of interest in this work. We introduce the language of manifolds, vector fields, Lie groups to more formally speak about configuration spaces of the robotic systems we are interested in. We then go on to review some aspects of differential geometry that play a role in our understanding of system mechanics. We then provide a basic review of Lagrangian mechanics and Lagrangian reduction via symmetry and nonholonomic momentum. Finally, we review the basics of inviscid fluid mechanics so we can study an ambient medium made up of point vortices in an otherwise irrotational flow.

2.1.1 Manifolds, Vector Fields, and Differential Forms

Manifolds. The dynamics of mechanical systems evolve on *manifolds*, requiring that we provide some definitions and introduce terminology so that these definitions may be unambiguously referred to throughout the document.

Definition 2.1.1 Homeomorphism *A continuous bijection $f : S \to T$ with a continuous inverse f^{-1} is called a homeomorphism. If such a map exists between sets S and T, S and T are homeomorphic.*

Should there not exist a homeomorphism between the entirety of sets S and T, it is still possible for these sets to be *locally homeomorphic*, meaning there exists a map f such that every point $P \in S$ has a neighborhood $U \subset S$ such that $f(U)$ is an open set in T. In this work, we are interested in *smooth* manifolds. That is, we are interested in manifolds for which there exists, at least in a local sense, a differentiable homeomorphism with a differentiable inverse. For the purposes of this document, a manifold can be defined as follows.

Definition 2.1.2 Manifold. *A manifold is a topological space that is locally homeomorphic to $\mathbb{R}^n$.*

This thesis concerns itself specifically with systems for which the dynamics evolve on *smooth* manifolds. This necessitates a short introduction of *coordinate charts* and coverings of coordinate charts. A coordinate chart on an n-dimensional manifold M is a set in that manifold $U \subset M$ together with a homeomorphism $\phi : U \to \phi(U) \subset \mathbb{R}^n$. An *atlas* on M is a collection of coordinate charts that cover M. When two coordinate charts (u, ϕ) and (v, ψ) overlap, the *transition*

functions $\psi \circ \phi^{-1} : \phi(u \cap v) \to \psi(u \cap v)$ and $\phi \circ \psi^{-1} : \psi(u \cap v) \to \phi(u \cap v)$ are homeomorphisms between subsets of $\mathbb{R}^n$. We call a manifold with an atlas having transition functions which are infinitely differentiable *smooth*. We use the word *manifold* to mean *smooth manifold* throughout this document.

Let Q be a manifold and q an arbitrary point in Q. Since we are ultimately interested in ODEs comprising velocities at each point $q \in Q$, we require a geometric description of the spaces home to such velocities. These velocities can be thought of as lying in a copy of $\mathbb{R}^n$ attached to the manifold Q at point q. We refer to this copy of $\mathbb{R}^n$ as the *tangent space* at point q and denote it by T_qQ. The tangent space T_qQ is also a real vector space.

Vector Fields. Let $(q^1, q^2, \cdots, q^n)$ be coordinates on a configuration manifold Q. We will denote the unit vector in the q^i direction as $\frac{\partial}{\partial q^i}$. Vectors $v \in T_qQ$ can be generally written as

$$v = v^1 \frac{\partial}{\partial q^1} + \cdots + v^n \frac{\partial}{\partial q^n}.$$

Additionally, we take advantage of the Einstein summation convention, where a superscripted quantity succeeded by a subscripted quantity results in a summation. The above vector then is written in total as

$$v = v^i \frac{\partial}{\partial q^i}.$$

Definition 2.1.3 Vector Field. *A vector field W on a manifold Q is a map $W : Q \to TQ$ at each point $q \in Q$.*

Suppose Q is n-dimensional. The tangent bundle, TQ, is the $2n$-dimensional manifold comprising the manifold Q and all the tangent spaces T_qQ for all $q \in Q$.

2.1.2 Lie Groups and Lie Algebras

Lie Groups. A group is a set G together with some operation, say $\cdot$, such that

1. If $a, b \in G$, then $a \cdot b \in G$.
2. If $a, b, c \in G$, then $(a \cdot b) \cdot c = a \cdot (b \cdot c)$.
3. There exists an element $e \in G$ termed the *identity element* such that $a \cdot e = e \cdot a = a$ for every $a \in G$.
4. For any $a \in G$, there exists an element $a^{-1} \in G$ such that $a \cdot a^{-1} = e$.

A Lie group is a manifold for which the group operation is smooth. The Lie groups of interest in this thesis will primarily be $SE(2)$, $\mathbb{R}^2$, or Cartesian products thereof, together with matrix multiplication as the group operation. Such Lie groups are often termed *matrix Lie groups*. For $SE(2)$, matrix multiplication constitutes the composition of rigid planar motions.

If G is a Lie group and g, h are elements of G, we will sometimes use the symbol L to mean

$$gh = L_g h, \tag{2.1}$$

where L_g is left multiplication or left translation by g. In the above example, we say h undergoes left translation by g. Note that we will also use the symbol "L" to denote the Lagrangian for a mechanical system. The use of the symbol "L" in the context of left translation will always have a subscript associated with it to denote an operation.

Left-invariant Vector Fields. Let $g, h \in G$ be group elements where G is a Lie group with matrix multiplication as the group operation. We will say that a vector field W on G is *left invariant* if

$$T_h L_g W(h) = W(gh), \qquad \forall g \in G. \tag{2.2}$$

This just means that the vector field evaluated at the point corresponding to left translation of h by g is equivalent to the push forward of W under L_g evaluated at h. This thesis will primarily be interested in left-invariant vector fields on the tangent space of a system's configuration manifold.

Group Actions. Let Q be a manifold and G a Lie group. A *left action* of G on Q is a map $\Phi : G \times Q \to Q$ such that $\Phi(e, q) = q$ for all $q \in Q$ and such that

$$\Phi(g, \Phi(h, q)) = \Phi(gh, q) \tag{2.3}$$

for all $g, h \in G$ and $q \in Q$. We say that an action of G on Q is *free* if $\Phi(g, q) = q$ only when $g = e$. An action Φ of a Lie group G on a manifold Q defines a tangent lifted action, $T\Phi$, of G on TQ such that

$$T\Phi : G \times TQ \mapsto TQ : \big(g, (q, v)\big) \mapsto (\Phi(g, q), T_q\Phi(g, q)v) \tag{2.4}$$

where $v \in T_qQ$. The mapping $T_q\Phi(g, q)$ is the tangent map at a point q corresponding to the action of g on q. This will be particularly important when verifying the left invariance of a system's Lagrangian under the action of a group.

Lie Algebras. Let G be a Lie group with matrix multiplication as the group operation. We refer to T_eG as the tangent space at the identity of the Lie group G. Endowed with an operation termed the *Jacobi-Lie bracket*, we refer to T_eG as the *Lie algebra* of G and denote it by $\mathfrak{g}$. The Jacobi-lie bracket operation is defined as follows.

Definition 2.1.4 Jacobi-Lie Bracket. *Let X and Y be vector fields on a manifold M. An additional vector field, the Jacobi-Lie bracket denoted by $[X, Y]$, is defined by the operation*

$$[X, Y](f) = X(Y(f)) - Y(X(f)) \tag{2.5}$$

for all smooth functions f on M.

Vectors in T_eG correspond to left-invariant vector fields in G. This means we can define a bracket operation on T_eG that satisfies

$$[\xi, \eta]_{\mathfrak{g}} = [X_\xi, X_\eta]_e. \tag{2.6}$$

Note that we will not directly utilize the Jacobi-Lie bracket, but include it so as to thoroughly define the Lie algebra $\mathfrak{g}$. In practice, vectors lying in T_eG are often thought of as coordinate vectors corresponding to velocities in the body frame of a robotic vehicle. This is the sense in which we will refer to elements in $\mathfrak{g}$.

If G is a Lie group and $\mathfrak{g}$ the corresponding Lie algebra, the *exponential map*, $\exp : \mathfrak{g} \to G$, maps each vector $\xi \in \mathfrak{g}$ to the element of G obtained by flowing along the left-invariant vector field X_ξ, starting at the identity e, for one unit of time.

Infinitesimal Generators. Let $\Phi : G \times Q \to Q$ be an action of a Lie group G on a manifold Q corresponding to each element ξ of the Lie algebra $\mathfrak{g}$ associated with G. The *infinitesimal generator* of the action Φ associated with the Lie algebra element ξ is defined as

$$\xi_Q(q) = \frac{d}{d\epsilon}\bigg|_{\epsilon=0} \Phi(\exp(\epsilon\xi), q). \tag{2.7}$$

$\xi_Q(q)$ is the element of T_qQ corresponding to the vector field ξ_Q.

Orbits. The orbit of a point $q \in Q$ under actions by elements $g \in G$ is denoted

$$\text{Orb}(q) = \{gq : g \in G\}. \tag{2.8}$$

In this thesis, Lie groups G are often part of the configuration space of a mechanical system. The notation gq means that a group element g can act via matrix multiplication on elements q in the configuration manifold and only induce a change in the G part of the manifold. We will also be interested in the tangent space to orbit of actions of G on Q. The tangent space to the orbit of a group through a point q is

$$T_q\text{Orb}(q) = \{\xi_Q(q) | \xi \in \mathfrak{g}\}. \tag{2.9}$$

The tangent space to the orbit of the group action therefore comprises the set of infinitesimal generators on Q at point q.

Differential Forms. There exist two $n-$dimensional vector spaces attached to each point q in an $n-$dimensional manifold Q. One of these is the tangent space T_qQ and the other the *cotangent* space T_q^*Q. As coordinates $q^1, \cdots, q^n$ on Q yield a basis $\{\frac{\partial}{\partial q^1}, \cdots, \frac{\partial}{\partial q^n}\}$ on T_qQ, they also yield a basis $\{dq^1, \cdots, dq^n\}$ for T_q^*Q. A smooth field of cotangent vectors on a manifold is called a *one-form*. A one-form at any point Q accepts one tangent vector as an argument and returns a real number. This operation is often called the *natural pairing* and is defined as follows.

Definition 2.1.5 Natural pairing. *The natural pairing of a one-form α and a tangent vector v is given by*

$$\langle \alpha, v \rangle = \alpha_i v^i \tag{2.10}$$

where $v = v^i \frac{\partial}{\partial q^i}$ and $\alpha = \alpha_i dq^i$, and the Einstein summation convention is assumed. This can also be thought of in terms of column vectors and row vectors with elements in α comprising a row vector and elements in v comprising a column vector.

For each component dq^i of a one-form and each component $\frac{\partial}{\partial q^j}$ of a vector field, the natural pairing is computed following

$$\langle dq^i, \frac{\partial}{\partial q^j} \rangle = \delta^i_j = \begin{cases} 1 & \text{if } i = j, \\ 0 & \text{if } i \neq j \end{cases}. \tag{2.11}$$

In this thesis, the constraints imposed on a mechanical system at a point $q \in Q$ will be thought of as one-forms lying in the cotangent space T_q^*Q.

2.2 Mechanics

2.2.1 Lagrangian Mechanics

Given a configuration manifold Q with coordinates q^i, the tangent bundle TQ is home to *induced coordinates* $(q^i, \dot{q}^i)$. The Lagrangian for a mechanical system will be represented by a map $L : TQ \to \mathbb{R}$. For the purposes of this document, the Lagrangian for a mechanical system will always equate to the difference in its *kinetic energy* and *potential energy*. We will always use the variables T and V to represent the kinetic and potential energies, respectively.

Hamiltons Principle. Hamilton's principle is stated as

$$\delta \int_{t_i}^{t_f} L dt = \delta \int_{t_i}^{t_f} (T - V) dt = 0. \tag{2.12}$$

In the absence of nonconservative forces on a system, the above equation must be satisfied for time parameterized trajectories between points in a manifold Q. Curves in Q satisfy the *Euler-Lagrange equations*, given by

$$\frac{d}{dt}\frac{\partial L}{\partial \dot{q}^i} - \frac{\partial L}{\partial q^i} = 0. \tag{2.13}$$

Note that the $2n$ first-order ODEs on the tangent bundle TQ correspond to the second-order ODEs given by the Euler-Lagrange equations.

Fiber Derivative. Given a Lagrangian $L : TQ \to \mathbb{R}$, the fiber derivative of the Lagrangian is a map from the tangent bundle TQ to the cotangent bundle T^*Q and is denoted by $\mathbb{F}L : TQ \to T^*Q$ [38]. In the context of Lagrangian mechanics, the fiber derivative is given by

$$\mathbb{F}L(q^i, \dot{q}^i) = \left(q^i, \frac{\partial L}{\partial \dot{q}^i}\right). \tag{2.14}$$

For purposes of this thesis, it suffices to consider the fiber derivative as a mapping from coordinates $(q^i, \dot{q}^i)$ in the tangent bundle TQ to coordinates in the cotangent bundle, where coordinates in the cotangent bundle are given by $(q^i, \frac{\partial L}{\partial \dot{q}^i})$.

Nonholonomic Constraints. The mechanical systems discussed in this thesis exhibit constraints on their motion. In particular, these constraints are enforced through no-slip conditions on wheels capable of rolling, but unable to slip in the direction lateral to their forward rolling motion. In general, mechanical constraints on a system with a configuration $q \in Q$ take the form

$$w(q^1, \ldots, q^n, \dot{q}^1, \ldots, \dot{q}^n) = 0. \tag{2.15}$$

If Eq. 2.15 can be integrated to obtain an equivalent constraint

$$W(q^1, \ldots, q^n) = 0, \tag{2.16}$$

then Eq. 2.15 is said to be *integrable*, and thus *holonomic*. Constraints not satisfying this particular property of integrability are called *nonholonomic*. This thesis concerns itself with nonholonomic constraints.

2.2.2 Symmetry and Nonholonomic Reduction

Identifying conserved quantities in mechanical systems lends itself to the reduction tools we are ultimately interested in leveraging. In particular, Noether's theorem [39] states that continuous symmetries correspond to conserved quantities in a mechanical system. In this section, we introduce the terminology necessary to leverage symmetries in the reduction we employ for the mechanical systems studied later in the document.

Let G be a Lie group with a group action Φ which acts on the left of a manifold Q. A mechanical system exhibits a continuous symmetry when the tangent lifted action corresponding to the action Φ leaves the Lagrangian invariant. That is,

$$L(q, \dot{q}) = L(\Phi(g, q), T_q\Phi(g, q)\dot{q}). \tag{2.17}$$

Conserved quantities associated with continuous symmetries in this way are termed *momentum maps* [5].

Momentum Maps. Let v_q be a tangent vector at point q in the tangent space T_qQ. The momentum map corresponding to a continuous symmetry is computed thus:

$$\langle J(v_q), \xi \rangle = \langle \mathbb{F}L(v_q), \xi_Q(q) \rangle. \tag{2.18}$$

Define the ith component of the vector field ξ_Q as ξ_Q^i. We compute the momentum map with respect to coordinates q^i as

$$J = \frac{\partial L}{\partial \dot{q}^i}(\xi_Q)^i \tag{2.19}$$

where a summation over i is assumed. Note every vector field ξ_Q on TQ is associated with a component of the momentum map. Given the above definition, the evolution equations corresponding to the nonholonomic momenta are computed as

$$\dot{J} = \frac{\partial L}{\partial \dot{q}^i}\left[\frac{d\xi}{dt}\right]_Q^i. \tag{2.20}$$

We will utilize Eq. 2.20 in the sections that follow in order to provide proof of particular behaviors in this reduced space. We will ultimately be choosing the vector fields ξ_Q that span the intersection of the constraint distribution $\mathcal{D}_q$ and the tangent space to the orbit of the group action $T_q\text{Orb}(q)$. This means we will know how to compute the nonholonomic momentum, but will need to compute the Lie algebra element associated with ξ_Q to be able to compute the evolution equations (Eq. 2.20). Our process for determining the Lie algebra elements ξ for which the evolution equations are computed is as follows. Any vector field in $\mathcal{D}_q \cap T_q\text{Orb}(q)$ must be the ξ_Q for some Lie algebra element ξ. However, since the direction of the vector field varies with the point q, the expression for this Lie algebra element may depend on the coordinates on Q. We choose any such vector field and corresponding to it there exists a scalar quantity J, with units of momentum, which we call a component of the nonholonomic momentum. We choose as many independent such vector fields required to span $\mathcal{D}_q \cap T_q\text{Orb}(q)$. These vector fields determine a comprehensive decomposition of the nonholonomic momentum into such scalar components. Furthermore, if given the time histories of a comprehensive set of such scalar quantities, it is possible to reconstruct the time histories of all of the system's configuration variables, such that the set of ODEs governing the evolution of these components consitutes a reduced representation of the dynamics of the full system.

2.3 Inviscid Fluid Mechanics

Inviscid fluid mechanics is typically well-suited for applications involving interactions of solid bodies in incompressible fluids for which inertial forces dominate viscous forces. Such fluids are often termed *high Reynolds number* flows and account for phenomena like that of vorticity. In this thesis, we will study fluids which are incapable of exerting shear stress. Such fluids are called *inviscid* fluids and will play an important role in the latter part of this thesis, when the ambient medium with which agents interact allow for the generation of vortices. In this section, we introduce the mathematical tools that allow us to analyze the dynamics of solid bodies in the presence of point vortices.

Complex Potentials. For a two-dimensional inviscid fluid, a scalar-valued function exists comprising the velocity potential and the stream function called the *complex potential*. At each point $z = x + iy$, such a function is defined as

$$w = \phi + i\psi. \tag{2.21}$$

We require that the complex potential be *holomorphic*, or complex differentiable in a neighorhood of every point. The stream function is defined to be ψ and the velocity potential ϕ. The velocity of any point in the fluid domain can be computed by the gradient of the complex potential. That is, at any point in the fluid domain, the velocity of that point is given by

$$\frac{dw}{dz} = u - iv, \tag{2.22}$$

where $u = \frac{d\phi}{dx} = \frac{d\psi}{dy}$ and $v = \frac{d\phi}{dy} = -\frac{d\psi}{dx}$. The stream function is constant along streamlines for the flow, which are everywhere orthogonal to lines of equal velocity potential. Complex potential functions for a desired flow can be written as a superposition of the individual flow contributions. For a system of a cylinder in the presence of point vortices, we can consider a complex potential function for the cylinder and a complex potential function for the point vortices separately. Their sum will constitute the complex potential for the flow we are interested in studying.

Circular Cylinders and Image Systems. The solid bodies we will study in this thesis can be modeled by appropriate placement of vortices that ensure the fluid flow is tangent to the boundary of the solid body at every point along the boundary of the body. These vortices are called *image vortices*. Let a complex potential for N vortices in an inviscid fluid be

$$w_v(z) = -\sum_{i=1}^{N} \Gamma_i \log(z - z_i) \tag{2.23}$$

where z_i is the location of the ith vortex and Γ_i is its strength. We use the variable w to denote a complex potential and a subscript of v to indicate a vortex. In seeking to eventually investigate the interactions of point vortices with a circular cylinder, we model the solid body of the cylinder by incorporating the appropriate *image system*. The complex potential for N vortices in the presence of a circular cylinder is

$$w(z) = -\sum_{i=1}^{N} \Gamma_i \log(z - z_i) - \Gamma_i \log(z - \frac{R^2}{z_i}) + \Gamma_i \log(z). \tag{2.24}$$

The image system comprises the final two terms in the above equation and nullifies the flow in a way that generates a circular cylinder with radius R. The image system effectively ensures the vectors in the flow are everywhere tangent to the boundary of a circular cylinder of radius R.

Chapter 3

The Chaplygin Beanie Atop a Compliant Platform

We consider the Chaplygin beanie[1] as our motivating example — effectively a Chaplygin sleigh with a rotor atop its body — coupled to a translationally compliant platform through a nonholonomic constraint on its wheel, shown in Fig. 3.1. We first consider the dynamics of the entire system to evolve only under its passive dynamics, i.e., there is no actuation in either the Chaplygin beanie or the platform atop which it sits. We develop the dynamics for this system using the method of nonholonomic reduction and prove that given a nonzero initial deformation in the spring coupling the vehicle's rotor to its body, the dynamics are asymptotically stable, with all of the system's angular momentum being converted into forward translational momentum. This stable behavior is likened to situations where a biological agent may prefer to relieve itself of actuation, taking advantage of its compliance and interactions with its environment to locomote.

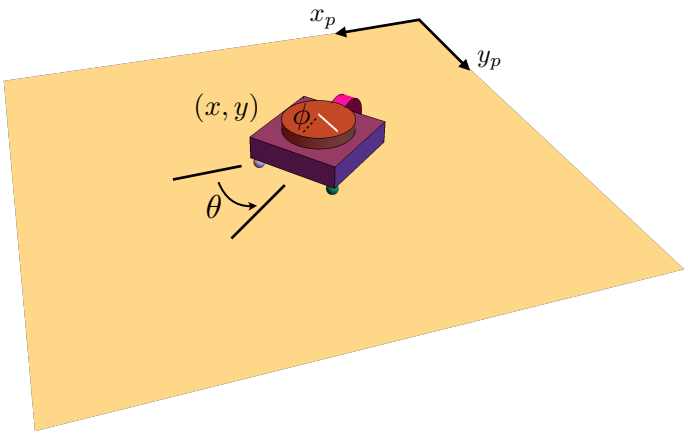

Figure 3.1: A Chaplygin beanie atop a translationally compliant platform. The vehicle's rotor angle relative to the heading is shown as ϕ, its heading as θ, its position relative to the platform as (x, y), and the position of the platform in a world frame, (x_p, y_p).

We begin by developing a dynamic model for an entirely passive system, consisting of a passive vehicle atop a platform with finite inertia. The Chaplygin beanie will serve as our passive vehicle,

[1] See [7] for the appropriate etymology of the Chaplygin beanie.

equipped with a linear torsional spring coupling its rotor to its body. Initial displacements of the rotor relative to the body result in motion of both the passive vehicle and the platform atop which it sits. Motions of the platform in this case are due to the forces arising through the no-slip constraint at the wheel of the Chaplygin beanie.

3.1 Nonholonomic Reduction

Constrained to the platform via a wheel located at its rear, the Chaplygin beanie locomotes using a rotor sitting atop its body. The total mass of the vehicle is represented by m, its rotational inertia about the center of mass as C, rotational inertia of the rotor about the center of mass as B, and the mass of the platform as M. The distance between the center of mass and the contact point at the wheel is denoted by a, and the stiffness of the spring coupling the rotor to the body denoted by k. The position of the vehicle relative to the platform is given coordinates (x, y), its orientation θ, the rotor angle relative to the vehicle heading by ϕ, and the position of the platform in a laboratory frame by (x_p, y_p). The evolution equations arising from the reduction are the changes in linear and angular momentum permitted by the no-slip constraint at the wheel and will replace the equations describing the evolution of $\dot{x}$, $\dot{y}$, and $\dot{\theta}$. The presence of a platform gives rise to two additional evolution equations, one of which is the time evolution of forward translational momentum of both the Chaplygin beanie and the platform, the second of which is the time evolution of the momentum of both the Chaplygin beanie and the platform in the direction orthogonal to that allowed by the no-slip consraint at the wheel. We also refer to this momentum term as momentum *lateral* to the forward motion of the vehicle. The Lagrangian for the system is given by

$$L = \frac{1}{2}m((\dot{x} + \dot{x}_p)^2 + (\dot{y} + \dot{y}_p)^2) + \frac{1}{2}C\dot{\theta}^2 + \frac{1}{2}B(\dot{\theta} + \dot{\phi})^2 + \frac{1}{2}M(\dot{x}_p^2 + \dot{y}_p^2) - \frac{1}{2}k\phi^2. \tag{3.1}$$

The nonholonomic constraint at the wheel is expressed as

$$-\dot{x}\sin\theta + \dot{y}\cos\theta - a\dot{\theta} = 0. \tag{3.2}$$

Constraints of this kind can also be thought of as one forms lying in the codistribution on the configuration manifold Q, written equivalently as

$$\omega = -\sin\theta dx + \cos\theta dy - ad\theta. \tag{3.3}$$

We require that the one form describing the no-slip constraint be annihilated by the system's generalized velocity, having coordinates $(x, y, \theta, \phi, x_p, y_p)$, at every point $q \in Q$. For the Chaplygin beanie on a platform with finite inertia, the manifold on which the dynamics evolve is described by the configuration manifold $Q = SE(2) \times \mathbb{S}^1 \times \mathbb{R}^2$. Note that both $SE(2)$ and $\mathbb{R}^2$ together with matrix multiplication as the group operation are both Lie groups, and that their Cartesian product will also yield a Lie group with matrix multiplication as the group operation. We let $G = SE(2) \times \mathbb{R}^2$ be the Lie group representing the group of rigid translations and rotations of the Chaplygin beanie and rigid translations of the platform. Let an arbitrary element of the Lie group G be described by $g = (x, y, \theta, x_p, y_p)$. Consider now a different element of G with assignment $g = (a, b, \alpha, c, d)$ and an element $q \in Q$ given by $q = (x, y, \theta, x_p, y_p, \phi)$. The left action of G on Q is given by

$$\begin{aligned}\Phi :& G \times Q \mapsto Q : (g, q) \mapsto (a + x\cos\alpha - y\sin\alpha, b + y\cos\alpha + x\sin\alpha,\\ & \theta + \alpha, c + x_p\cos\alpha - y_p\sin\alpha, d + y_p\cos\alpha + x_p\sin\alpha, \phi).\end{aligned} \tag{3.4}$$

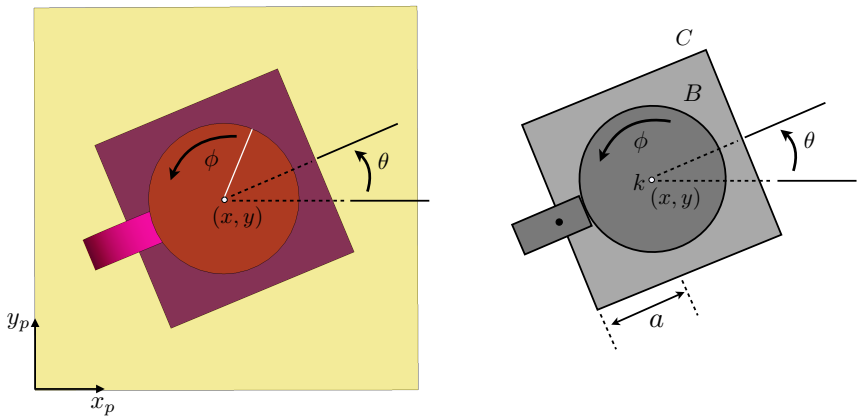

Figure 3.2: (Left) Two-dimensional diagram of a Chaplygin beanie on a platform with associated coordinates. (Right) Two-dimensional diagram of a Chaplygin beanie with parameter assignments.

The above defines a tangent lifted action, $T\Phi$, of G on the tangent bundle TQ, given by

$$T\Phi : G \times TQ \mapsto TQ : \big(g, (q, \dot{q})\big) \mapsto (\Phi(g, q), T_q\Phi(g, q)\dot{q}) \tag{3.5}$$

where $T_q\Phi(g, q)$ is given by

$$T_q\Phi(g, q) = \begin{bmatrix} \cos\alpha & -\sin\alpha & 0 & 0 & 0 & 0 \\ \sin\alpha & \cos\alpha & 0 & 0 & 0 & 0 \\ 0 & 0 & 1 & 0 & 0 & 0 \\ 0 & 0 & 0 & \cos\alpha & -\sin\alpha & 0 \\ 0 & 0 & 0 & \sin\alpha & \cos\alpha & 0 \\ 0 & 0 & 0 & 0 & 0 & 1 \end{bmatrix}. \tag{3.6}$$

$T_q\Phi(g, q)$ is also written as $T_q\Phi_g$. We can use the mapping of tangent vectors according to the above Jacobian to show that the Lagrangian, Eq. 3.1, is invariant under the tangent lifted action, Eq. 3.5. We must now verify the constraint one form, ω, is invariant under the group action, Φ. Given a point $q \in Q$ and a tangent vector $\dot{q} \in T_qQ$, we check for left-invariance by computing

$$< \omega_q, \dot{q} > = < \omega_{\Phi_g q}, T_q\Phi_g \dot{q} >, \tag{3.7}$$

where ω_q is the constraint one form evaluated at point q and $\omega_{\Phi_g q}$ is the constraint one form evaluated at point q after being mapped through the group action. The natural pairing above is computed as

$$\begin{bmatrix} -\sin\theta & \cos\theta & -a & 0 & 0 & 0 \end{bmatrix} \begin{bmatrix} \dot{x} \\ \dot{y} \\ \dot{\theta} \\ \dot{x}_p \\ \dot{y}_p \\ \dot{\phi} \end{bmatrix} = \begin{bmatrix} -\sin(\theta+\alpha) & \cos(\theta+\alpha) & -a & 0 & 0 & 0 \end{bmatrix} T_q\Phi_g \begin{bmatrix} \dot{x} \\ \dot{y} \\ \dot{\theta} \\ \dot{x}_p \\ \dot{y}_p \\ \dot{\phi}. \end{bmatrix} \tag{3.8}$$

Thus, the system's Lagrangian is invariant under the tangent lifted action, and the constraint one form is invariant under the cotangent lifted action, making G a symmetry group. The Lie

group $G = SE(2) \times \mathbb{R}^2$ then acts on the G part of Q via left translation, leaving the $\mathbb{S}^1$ part unchanged.

We take an approach presented in [8], involving the choosing of appropriate left-invariant vector fields spanning the intersection of the constraint distribution and the space tangent to the orbit of the group action, and leverage [7] in computing the components of the nonholonomic momentum. We designate the distribution $\mathcal{D}_q$ as the space of all tangent vectors which annihilate the constraint one form, ω, and is given by

$$\mathcal{D}_q = \text{span}\{-a\sin\theta\frac{\partial}{\partial x} + a\cos\theta\frac{\partial}{\partial y} + \frac{\partial}{\partial\theta}, \cos\theta\frac{\partial}{\partial x} + \sin\theta\frac{\partial}{\partial y}, \frac{\partial}{\partial\phi}\}. \tag{3.9}$$

Furthermore, we designate $T_q\text{Orb}(q)$ as the space tangent to the orbit of the group action, given by

$$T_q\text{Orb}(q) = \text{span}\{\frac{\partial}{\partial x}, \frac{\partial}{\partial y}, \frac{\partial}{\partial\theta}, \frac{\partial}{\partial x_p}, \frac{\partial}{\partial y_p}\}. \tag{3.10}$$

We then choose appropriate vector fields on the configuration space, Q, to span

$$S_q = \mathcal{D}_q \cap T_q\text{Orb}(q), \quad \forall q \in Q. \tag{3.11}$$

The intersection of $\mathcal{D}_q$ and $T_q\text{Orb}(q)$ constitutes the space in which a reduced representation of the dynamics evolve. Its dimension corresponds to the number of evolution equations obtained from the reduction. The following choice of vector fields is made to define this intersection.

$$\begin{aligned} S_q = \text{span}\{&-a\sin\theta\frac{\partial}{\partial x} + a\cos\theta\frac{\partial}{\partial y} + \frac{\partial}{\partial\theta}, \cos\theta\frac{\partial}{\partial x} + \sin\theta\frac{\partial}{\partial y}, \\ &\cos\theta\frac{\partial}{\partial x_p} + \sin\theta\frac{\partial}{\partial y_p}, -\sin\theta\frac{\partial}{\partial x_p} + \cos\theta\frac{\partial}{\partial y_p}\}. \end{aligned} \tag{3.12}$$

The first two vector fields correspond to rotation about the contact point at the wheel and longitudinal translation of the vehicle, respectively [7]. Flow along the third corresponds to forward translation of the entire system, including the platform, along the forward direction of the Chaplygin beanie. The fourth of these vector fields represents motions of the entire system lateral to the forward direction of the Chaplygin beanie.

We invoke the Einstein summation convention in the following definition of the momentum map and designate q^i as the ith coordinate on the configuration manifold, Q. The nonholonomic momenta are computed following

$$J^{nhc} = \frac{\partial L}{\partial\dot{q}^i}(\xi_Q)^i. \tag{3.13}$$

The resulting momenta are given directly by (3.14). It is clear by inspection that J_{LT} and J_{RW} correspond to forward translational momentum and angular momentum about the contact point of the wheel, respectively. The quantities J_X and J_Y correspond to forward translational momentum and momentum lateral to the direction allowed by the nonholonomic constraint for both the Chaplygin beanie and the platform.

$$
\begin{aligned}
J_{LT} &= m(\dot{x}+\dot{x}_p)\cos\theta + m(\dot{y}+\dot{y}_p)\sin\theta,\\
J_{RW} &= -ma(\dot{x}+\dot{x}_p)\sin\theta + ma(\dot{y}+\dot{y}_p)\cos\theta\\
&\quad + (B+C)\dot{\theta} + B\dot{\phi},\\
J_X &= m(\dot{x}+\dot{x}_p)\cos\theta + m(\dot{y}+\dot{y}_p)\sin\theta +\\
&\quad M\dot{x}_p\cos\theta + M\dot{y}_p\sin\theta,\\
J_Y &= -m(\dot{x}+\dot{x}_p)\sin\theta + m(\dot{y}+\dot{y}_p)\cos\theta -\\
&\quad M\dot{x}_p\sin\theta + M\dot{y}_p\cos\theta.
\end{aligned}
\tag{3.14}
$$

The evolution equations are computed following (3.15) and are given by (3.16), shown below.

$$
\dot{J}^{nhc} = \frac{\partial L}{\partial \dot{q}^i}\left[\frac{d\xi}{dt}\right]_Q^i \tag{3.15}
$$

$$
\begin{aligned}
\dot{J}_{LT} &= -\frac{m((B+C)J_Y + Ma(J_{RW}-B\alpha))(maJ_Y - (m+M)(J_{RW}-B\alpha))}{(M(ma^2+B+C)+m(B+C))^2},\\
\dot{J}_{RW} &= \frac{aJ_{LT}(maJ_Y - (m+M)(J_{RW}-B\alpha))}{M(ma^2+B+C)+m(B+C)},\\
\dot{J}_X &= -\frac{J_Y(maJ_Y + (m+M)(J_{RW}-B\alpha))}{M(ma^2+B+C)+m(B+C)},\\
\dot{J}_Y &= -\frac{J_X(-maJ_Y + (m+M)(J_{RW}-B\alpha))}{M(ma^2+B+C)+m(B+C)}
\end{aligned}
\tag{3.16}
$$

The long-term behavior for this system under arbitrary initial ϕ is stable, with J_{LT} tending to a constant value while J_{RW} and ϕ tend to zero, as shown in Fig. 3.3.

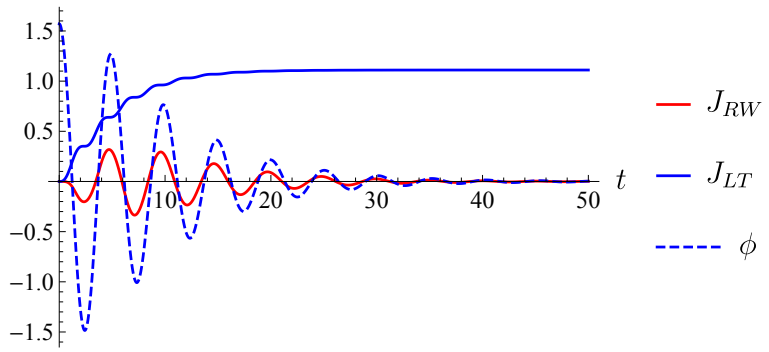

Figure 3.3: Rotational momentum about the rear wheel, longitudinal translational momentum, and the rotor angle

3.2 Stability

In this section, we present a formal argument for stable behaviors of this kind under the assumption that the system dynamics evolve on the zero level set of momentum, that is, any

initial condition for which $J_X^2 + J_Y^2 = 0$. Defining the following variables, the nonholonomic momenta, ϕ, and $\dot{\phi}$ can be expressed as

$$r = \frac{J_{LT}}{d}, \quad w = \frac{J_{RW} - B\alpha}{d}, \quad p_x = \frac{J_X}{d}, \\ p_y = \frac{J_Y}{d}, \quad \alpha = \dot{\phi}. \tag{3.17}$$

The constants $d = m(B+C) + M(ma^2 + B + C)$, $\gamma_1 = -m^2a(B+C)/d$, $\gamma_2 = (m(m+M)(B+C) - m^2Ma^2)/d$, $\gamma_3 = mMa(m+M)/d$, $\lambda_1 = ma^2$, $\lambda_2 = -a(m+M)$, $\mu_1 = -ma$, $\mu_2 = m+M$, $\nu_0 = B/d$, $D = B(mMa^2 + C(m+M))$, $\nu_1 = -dk/D$, $\nu_2 = -Bma^2(m+M)/(dD)$, $\nu_3 = aB(m+M)^2/(dD)$, $\nu_4 = Bm^2a^2/(dD)$, and $\nu_5 = -mBa(m+M)/(dD)$ fully encapsulate the presence of system parameters in a more convenient form for analysis. The reduced dynamics are then easier to analyze for stability. Taking the time derivatives of (3.17) and using (3.16) to make the necessary substitutions, the evolution equations become

$$\begin{aligned} \dot{r} &= \gamma_1 p_y^2 + \gamma_2 p_y w + \gamma_3 w^2, \\ \dot{w} &= \lambda_1 r p_y + \lambda_2 r w - \nu_0(\nu_1\phi + \nu_2 r p_y + \nu_3 r w + \nu_4 p_x p_y + \nu_5 p_x w), \\ \dot{p}_x &= \mu_1 p_y^2 + \mu_2 p_y w, \\ \dot{p}_y &= -\mu_1 p_x p_y - \mu_2 p_x w, \\ \alpha &= \dot{\phi}, \\ \dot{\alpha} &= \nu_1\phi + \nu_2 r p_y + \nu_3 r w + \nu_4 p_x p_y + \nu_5 p_x w. \end{aligned} \tag{3.18}$$

The dynamics given by (3.18) can be further simplified under assumptions of momentum conservation. The quantity $p_x^2 + p_y^2$ is conserved, with all its level sets invariant under (3.18). We wish to prove that all trajectories corresponding to $p_x^2 + p_y^2 = 0$ approach the r axis asymptotically. Restricting the dynamics to this level set, (3.18) can be written as

$$\dot{r} = \gamma_3 w^2, \quad \dot{w} = \lambda_2 r w - \nu_0(\nu_1\phi + \nu_3 r w), \\ \dot{p}_x = 0, \quad \dot{p}_y = 0, \quad \alpha = \dot{\phi}, \\ \dot{\alpha} = \nu_1\phi + \nu_3 r w. \tag{3.19}$$

The time evolution of r, w, ϕ, and α then fully describe the behavior of the system. By inspection it is clear that $\dot{r}$ is nonnegative, and is positive where w is nonzero. For $w = 0$, $\dot{w}$ is nonzero for $\phi \neq 0$. It follows that r will increase for all time given that $w \neq 0$ and $\phi \neq 0$. Thus, r will increase for all time unless w, ϕ, and α, are zero for all time, requiring r to increase unless the flow of the vector field corresponding to (3.19) is always on the r axis. All fixed positive values of r correspond to a linear dynamical system described by $\dot{w}$, α, and $\dot{\alpha}$. For every such r, denoted by r_c, the dynamics are then

$$\begin{bmatrix} \dot{w} \\ \alpha \\ \dot{\alpha} \end{bmatrix} = \begin{bmatrix} \lambda_2 r_c w - \nu_0(\nu_1\phi + \nu_3 r_c w) \\ \dot{\phi} \\ \nu_1\phi + \nu_3 r_c w \end{bmatrix}. \tag{3.20}$$

The Jacobian of (3.20) is

$$A = \begin{bmatrix} \lambda_2\nu_0\nu_3 r_c & -\nu_0\nu_1 & 0 \\ 0 & 0 & 1 \\ \nu_3 r_c & \nu_1 & 0 \end{bmatrix}. \tag{3.21}$$

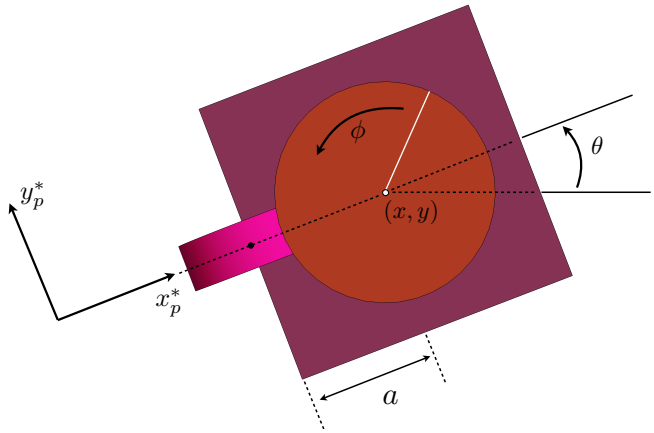

Figure 3.4: Platform actuation rotated so as to exert control in the direction orthogonal to direction of motion allowed by the no-slip constraint at the wheel

The eigenvalues of (3.21) at $(w, \phi, \alpha) = (0, 0, 0)$ correspond to the roots of a third order polynomial in p with parameter-dependent coefficients, written as

$$p^3 + (\nu_0\nu_3 r_c - \lambda_2 r_c)p^2 - \nu_1 p + \lambda_2\nu_1 r_c = 0. \tag{3.22}$$

With $r_c > 0$, the polynomial above has roots with all negative real part, showing that w, ϕ, and α exponentially decrease to zero as r increases. This result suggests a stable fixed point of (3.19) at $(r, w, \phi, \alpha) = (r_\infty, 0, 0, 0)$ given knowledge of the asymptotic values of w, ϕ, and α. Since the dynamics are energy-conserving, the initial and final energies of the system must be equal, with the asymptotic value of r for the case where the system is initially at rest calculated as

$$r_\infty = \lim_{t\to\infty} r = \frac{\phi(0)}{d}\sqrt{\frac{kmM}{m+M}}.$$

It follows that the asymptotic value of r can be determined for any initial conditions corresponding to the system being initially at rest. Of considerable note is the linear relationship between r_∞ and the initial rotor angle relative to the body of the Chaplygin beanie, i.e., the initial spring deformation.

3.3 Exogenous Control

Coordination of biological agents in fluids or compliant substrates is often accomplished by the agent taking actions based on locally-sensed dynamics of their environment. Though agents take such actions, they also relieve themselves of their actuation under some circumstances, remaining passively compliant for some time in their environment before taking up actuation again. Such passivity has proven useful for achieving meaningful locomotive behaviors [14]. Prior works have considered this problem in the context of vibrational entrainment of passively compliant Chaplygin beanies atop an actuated platform [2]. In this section, we study the Chaplygin beanie atop an actuated platform and ask whether the system can be excited so as to induce predictable locomotion. We investigate this problem from a perspective of exogenous control, i.e., we excite the platform in an oscillatory manner, uncaring of *where* the control originates, and characterize motion primitives for a passively compliant Chaplygin beanie as it responds passively to its environment.

3.3.1 Frequency Response Analysis

We seek to characterize locomotive behaviors when the frequency at which the environment is stimulated varies over a range of values containing the natural frequency of the rotor and the modal frequency of the body-rotor couple when not constrained to the platform, both of which are dependent on the stiffness of the spring. Consider a single passively compliant Chaplygin beanie atop an actuated platform and let its parameters, m, B, C, a, and k, be equal to unity. Note that the platform can only be actuated in the directions (x_p, y_p) as shown in Fig. 3.2. There's no reason to assume a relationship exists between forward translational speed, heading, or even stability, when actuating purely in the (x_p, y_p) directions. In fact, such a relationship is obfuscated by dependence on the initial heading of the vehicle. However, such a relationship could exist when considering actuation in a rotated frame of reference, orthogonal to the allowable direction of motion required by the nonholonomic constraint at the vehicle's wheel.

Fig. 3.4 shows the rotated reference frame of the platform. Actuation along y_p^* is not only independent of the heading of the vehicle, but also the direction for which its passive dynamics are most responsive. Actuation along x_p^*, for example, causes no deformations of the rotor relative to the body and therefore no passive response. Consider the natural frequency of the rotor and the modal frequency of the vehicle when not constrained to the platform, given by

$$\omega_{nat} = \sqrt{\frac{k}{B}}, \qquad \omega_{mod} = \sqrt{\frac{k(B+C)}{BC}}. \tag{3.23}$$

With a spring coupling the cart to the rotor, we sweep through a range of frequencies for a particular set of parameters to analyze the response of the system to exogenous forcing in the y_p^* direction and use asymptotic mean forward translational velocity as a performance metric. However, under certain periodic actuation the system will approach persistently undulatory behavior, requiring that we consider the mean velocity for an integer number of periods of oscillation. Forward translational velocity in the body frame of the vehicle is given by

$$\xi_x = \dot{x}\cos\theta + \dot{y}\sin\theta.$$

The above is equivalent to the velocity in the direction allowable by the nonholonomic constraint on the wheel. Consider a situation that allows the orientation of the agent to be tracked in the environment. We actuate the platform according to

$$\begin{bmatrix} x_p^* \\ y_p^* \end{bmatrix} = \begin{bmatrix} \cos\theta & -\sin\theta \\ \sin\theta & \cos\theta \end{bmatrix}^{-1} \begin{bmatrix} x_p \\ y_p \end{bmatrix} \tag{3.24}$$

and let $x_p^* = 0$ and $y_p^* = A\sin(\omega t)$. Note that this is effectively a feedback-like controller in that it requires tracking the heading of the vehicle, which is then used to compute the control y_p^*. Setting system parameters and the amplitude A to unity, we discretize the range of frequencies between 0.1 and 2.0 into $N = 70$ equally-spaced intervals. Using the final three periods of oscillation to compute the mean forward translational velocity, denoted by $\bar{\xi}_x$, we obtain the frequency response plot shown in Fig. 3.5.

In carrying out this experiment, it is clear that the natural frequency of the rotor and modal frequency of the system in free space bound a region of high performance when considering mean forward translational velocity as a metric. Additional questions concerning generalizability and associated behaviors arise from this particular result. To address the first of these questions, we vary the parameters for the vehicle, compute the corresponding frequencies given in (3.23)

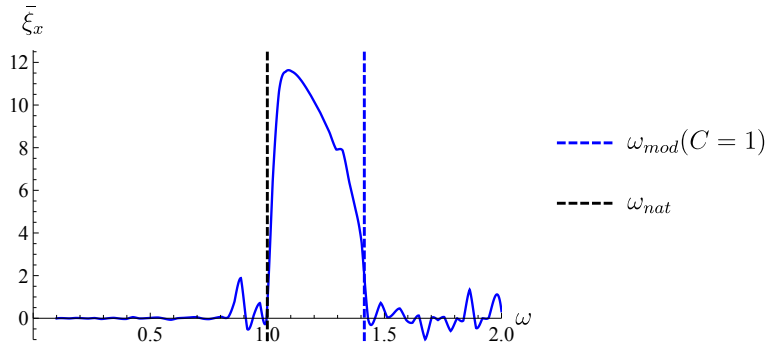

Figure 3.5: Frequency response of a passive Chaplygin beanie under external actuation in the body frame. The parameters were set to unity to obtain this response.

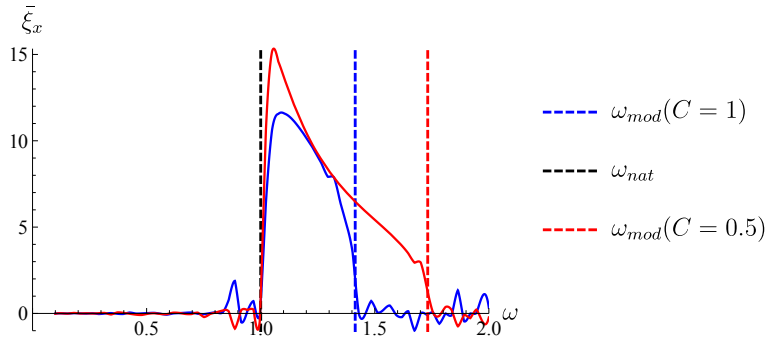

Figure 3.6: Frequency responses of a Chaplygin beanie for two different parameter combinations

and generate similar results to Fig. 3.5. The results of these experiments are shown in Fig. 3.6. The natural frequency of the rotor and modal frequency of the vehicle in free space again yield lower and upper bounds on regions of high performance.

Of further interest are behaviors emerging from actuating within, and outside of, the frequency bounds set by (3.23). In particular, we wish to characterize the frequencies that result in stable dynamics and from that characterization deduce motion primitives for controlling multiple passive vehicles. An analysis of the time evolution of θ when actuating the platform at frequencies inside and oustide of the bands given above is shown in Fig. 3.7, clarifying the existence of distinct dynamics in the vehicle's heading. The blue curve visible in Fig. 3.7 is actually a family of curves all resulting from frequencies lying within the bounds of the natural and modal frequency of the vehicle, all resembling stable oscillatory behavior. The red and green curves each correspond to θ dynamics of a single frequency chosen that satisfies the inequalities shown in the legend.

3.3.2 Manipulation

The frequency characterization in 3.3.1 provides clear rules by which we can exert control over the platform to manipulate Chaplygin beanies. Actuating the platform at frequencies within the bounds set by the natural frequency of the rotor and the modal frequency of the vehicle in free space allow for control primitives which induce vehicles to achieve stable undulatory locomotion along a particular heading. We term such behavior in the context of manipulating multiple agents as *dispersion*. Actuation outside of these boundaries yield trajectories corresponding to much more complex dynamics, not as easily classified as those of stable undulatory behavior. We discuss some of these behaviors in Section **??**. Two such trajectories are shown in Fig. 3.8.

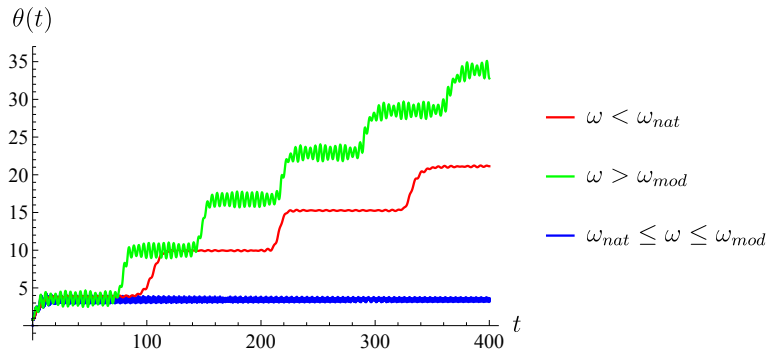

Figure 3.7: Analysis of the asymptotic heading of a Chaplygin beanie over the actuation bounds described in Fig. 3.5

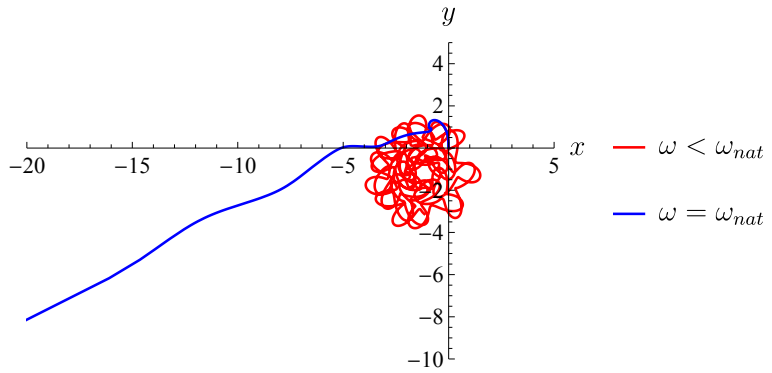

Figure 3.8: Trajectories of two individual simulations for actuation of the platform inside of the bounds (blue) and outside of bounds (red) defined by ω_{nat} and ω_{mod}

The beanie under external actuation with $\omega = \omega_{nat}$ will disperse from its initial position and undulate stably at a particular heading for all time. The degree to which it stably oscillates in θ increases with increasing ω, as long as actuation stays within the bounds of the natural frequency of the rotor and the modal frequency of the vehicle. Though no formal guarantee is given in this work, the authors assert that trajectories corresponding to those of platform actuation at frequencies of $\omega < \omega_{nat}$ or $\omega > \omega_{mod}$ will stay within some neighborhood of its initial position, much like that of the red trajectory in Fig. 3.8. Such trajectories are also prone to exhibit dynamics that reveal the presence of multi-scale time dynamics, discussed below.

This result clarifies the ability to control passive vehicles using the kind of actuation given by (3.24). Consider a case with two identical passive Chaplygin beanies at rest atop an actuated platform with different initial headings. Naively assuming control over the platform to manipulate one vehicle in this sense does not guarantee a certain behavior for the other. In the presence of other passive vehicles, however, to achieve a desired behavior, the platform can be actuated corresponding to the desired control for that particular vehicle and its resulting behavior remains independent of the others. Fig. 3.9 shows such a case if the desired behavior for beanie 1 is to stay within some neighborhood of its initial position.

Though beanie 2 appears to stably locomote away in this example, there is no basis in assuming it does so. Similarly, actuation within the frequency bands discussed above would result in the vehicle approaching a stable oscillatory trajectory rather than oscillating about the initial position. In this result, we emphasize the importance of exerting control over a particular agent in a multi-agent setting given that we actuate the platform according to (3.24). The

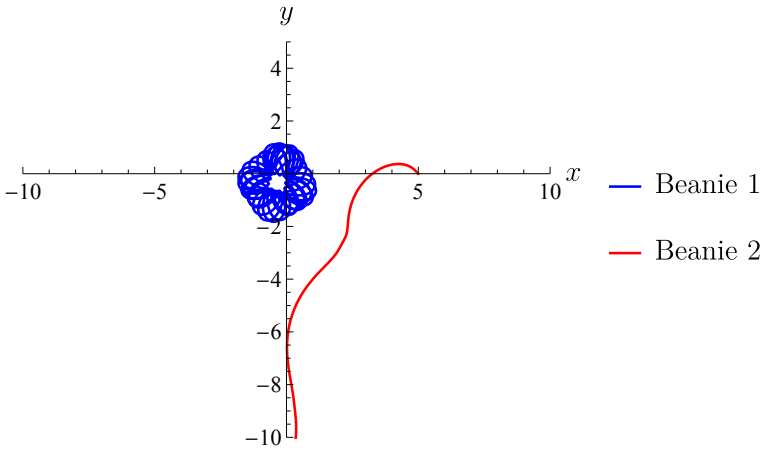

Figure 3.9: Resulting trajectories for two Chaplygin beanie agents atop an actuated platform. The blue trajectory corresponds to actuation of beanie 1 at a frequency lower than the natural frequency of its rotor. The red trajectory corresponds to the dynamics induced by actuating the platform so as to induce the behavior seen in beanie 1.

ability to actuate the platform in this way leads to questions concerning the control of multiple agents. Naively, one may conclude this control methodology can be targeted to one agent and switched at any time to target another to disperse or station-keep agents as needed, but this is nullified by each vehicle having attained nonzero momentum.

3.4 Summary and Future Work

We first developed the reduced equations for a system consisting of a passively compliant Chaplygin beanie atop a translationally compliant platform with finite inertia and proved that for trajectories corresponding to $p_x^2 + p_y^2 = 0$, the system is stable for arbitrary initial conditions in ϕ. We then established a characterization for control of a multi-vehicle system coupled dynamically to a medium that gives rise to rich dynamical behavior. Though it is clear based on the present work that there exist parameter-invariant bounds on platform actuation frequencies for achieving stable undulatory behavior of a passive vehicle under exogenous control, formal proof for this result is sought. Other interesting phenomena are exhibited by the nonlinear dynamics that warrant further exploration. Namely, certain platform actuation frequencies yield behaviors which indicate the presence of multi-scale time dynamics, demonstrated in Fig. 3.10. This behavior relates qualitatively to that exhibited by a three-link snake-like robot in [40].

The system was given an initial position at the origin and controlled corresponding to (3.24). The vehicle locomotes away along some heading for some time, reverses direction, locomotes for some time, switches its heading, and repeats this behavior. The dynamics of moving along in some heading occur at a fast time scale, while the dynamics for switching direction occur at a much slower time scale. Changes in the direction taken by the vehicle likely correspond to bifurcations in the dynamics at one of these time scales, the analysis of which is a topic of future work. The actuated system has also been shown to display stable oscillatory behavior for frequencies within the frequency bands discussed. As such, proving stabilizability for the controlled system will also be included in future publications.

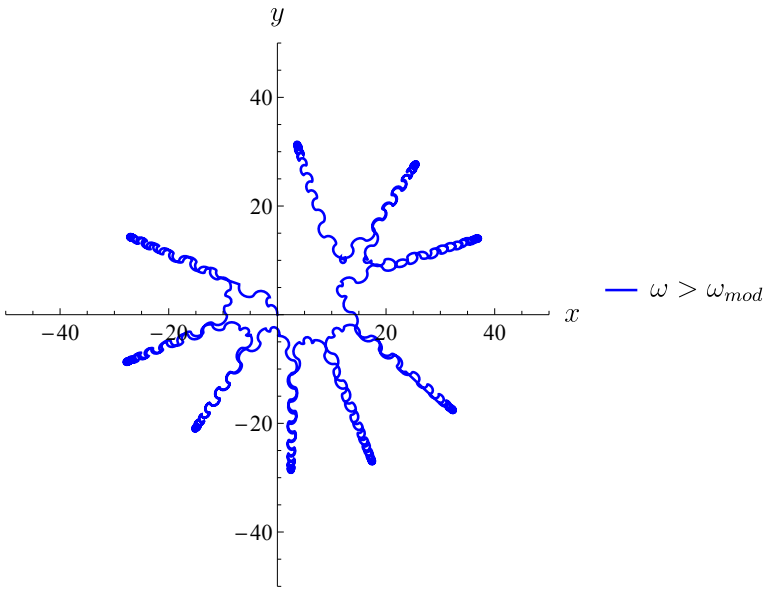

Figure 3.10: Trajectory resulting from actuating the platform at a frequency of $\omega < \omega_{mod}$ for a Chaplygin beanie with parameters $C = 0.5$, $m = B = k = 1$ for a duration of 500 simulation seconds.

Chapter 4

Two Chaplygin Beanies Atop a Compliant Platform

The preceding chapter developed a reduced representation for the dynamics of a *single* Chaplygin beanie on a movable platform, permitting a more rigorous analysis of behaviors arising from its passive dynamics. We then provided some preliminary results of the exogenous control of two passive Chaplygin beanies on an actuated platform using motion primitives deduced from the characterization of their frequency response. In this chapter, we develop the reduced dynamics for two Chaplygin beanies on a movable platform and investigate their passive dynamics in a reduced space.

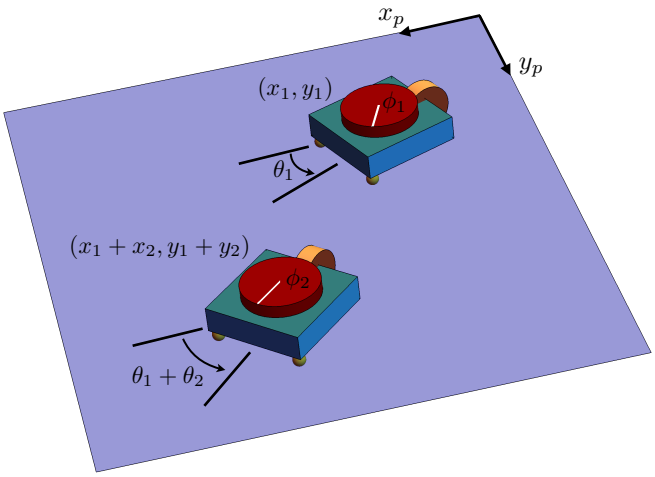

Figure 4.1: Two Chaplygin beanies atop a translationally compliant platform. Vehicle rotor angles relative to the heading are shown as ϕ_i, headings as θ_i, positions relative to the platform as (x_i, y_i), and the position of the platform in a world frame, (x_p, y_p).

4.1 Nonholonomic Reduction

Like the preceding case involving a single Chaplygin beanie, each of the two Chaplygin beanies is constrained to the platform via a wheel located at its rear, shown in orange in Fig. 4.1. Their individual masses are denoted m_i where i is used to denote the ith agent. The rotational inertia about an agent's center of mass is represented by C_i, the rotational inertia of its rotor by B_i,

the distance from the wheel and the center of its body by a_i, and the stiffness of the spring coupling the cart to its rotor by k_i. The mass of the platform is still given by M. The position and orientation of the second agent is specified relative to the first agent as shown in Fig. 4.1. The Lagrangian for this particular choice of coordinates is written as

$$\begin{aligned} L = &\frac{1}{2}m_1((\dot{x}_1+\dot{x}_p)^2+(\dot{y}_1+\dot{y}_p)^2)+\frac{1}{2}m_2((\dot{x}_1+\dot{x}_2+\dot{x}_p)^2+(\dot{y}_1+\dot{y}_2+\dot{y}_p)^2)\\ &+\frac{1}{2}M\dot{x}_p^2+\frac{1}{2}M\dot{y}_p^2+\frac{1}{2}C_1\dot{\theta}_1^2+\frac{1}{2}C_2(\dot{\theta}_1+\dot{\theta}_2)^2+\frac{1}{2}B_1(\dot{\theta}_1+\dot{\phi}_1)^2+\frac{1}{2}B_1(\dot{\theta}_1+\dot{\theta}_2+\dot{\phi}_2)^2\\ &-\frac{1}{2}k_1\phi_1^2-\frac{1}{2}k_2\phi_2^2. \end{aligned} \tag{4.1}$$

There exist two constraints on this system: one for the no-slip condition at the wheel of each Chaplygin beanie. These nonholonomic constraints are equivalent to two one-forms on the cotangent space

$$\omega_1 = -\sin\theta_1 dx_1+\cos\theta_1 dy_1-a_1 d\theta_1, \tag{4.2}$$

$$\omega_2 = -\sin(\theta_1+\theta_2)d(x_1+x_2)+\cos(\theta_1+\theta_2)d(y_1+y_2)-a_2 d(\theta_1+\theta_2). \tag{4.3}$$

The dynamics of two Chaplygin beanies on a movable platform evolve on the manifold $Q = SE(2)\times\mathbb{S}^1\times SE(2)\times\mathbb{S}^1\times\mathbb{R}^2$. We again require that the one-form describing these no-slip constraints be annihilated by the generalized velocity at every point $q = (x_1, y_1, \theta_1, \phi_1, x_2, y_2, \theta_2, \phi_2, x_p, y_p)\in Q$. Much like an $\mathbb{R}^2$ symmetry arises from the assignment of a single beanie relative to the platform, so too does an $\mathbb{R}^2$ symmetry arise from assigning the second beanie relative to the first beanie. One might suspect another $SE(2)$ symmetry to exist, however, the presence of an additional orientation variable — θ_2 — precludes this. Despite this break in symmetry, we can still seek to reduce out x_1, y_1, θ_1, x_2, y_2, x_p, and y_p, replacing them with six momentum variables. For the Lie group $G = SE(2)\mathbb{R}^2\times\mathbb{R}^2$, let a generic group element be represented by $g = (\bar{x}_1, \bar{y}_1, \bar{\theta}_1, \bar{x}_2, \bar{y}_2, \bar{x}_p, \bar{y}_p)$. The Lie group G acts on Q via left translation, leaving ϕ_1, ϕ_2, and θ_2 unchanged. We write the group action Φ as

$$\begin{aligned} \Phi :&G\times Q\mapsto Q : (g,q)\mapsto(\bar{x}_1+x_1\cos\alpha_1-y_1\sin\alpha_1, \bar{y}_1+y_1\cos\alpha_1+x_1\sin\alpha_1, \theta_1+\alpha_1,\\ &\phi_1, \bar{x}_2+x_2\cos\alpha_1-y_2\sin\alpha_1, \bar{y}_2+y_2\cos\alpha_1+x_2\sin\alpha_1,\\ &\theta_2, \phi_2, \bar{x}_p+x_p\cos\alpha_1-y_p\sin\alpha_1, \bar{y}_p+y_p\cos\alpha_1+x_p\sin\alpha_1). \end{aligned} \tag{4.4}$$

The tangent part of the lifted action corresponding to the above group action is

$$T_q\Phi(g,q) = \begin{bmatrix} \cos\alpha_1 & -\sin\alpha_1 & 0 & 0 & 0 & 0 & 0 & 0 & 0 & 0\\ \sin\alpha_1 & \cos\alpha_1 & 0 & 0 & 0 & 0 & 0 & 0 & 0 & 0\\ 0 & 0 & 1 & 0 & 0 & 0 & 0 & 0 & 0 & 0\\ 0 & 0 & & & & & & & & \\ 0 & 0 & 0 & 1 & 0 & 0 & 0 & 0 & 0 & 0\\ 0 & 0 & & & & & & & & \\ 0 & 0 & 0 & 0 & \cos\alpha_1 & -\sin\alpha_1 & 0 & 0 & 0 & 0\\ 0 & 0 & & & & & & & & \\ 0 & 0 & 0 & 0 & \sin\alpha_1 & \cos\alpha_1 & 0 & 0 & 0 & 0\\ 0 & 0 & & & & & & & & \\ 0 & 0 & 0 & 0 & 0 & 0 & 1 & 0 & 0 & 0\\ 0 & 0 & & & & & & & & \\ 0 & 0 & 0 & 0 & 0 & 0 & 0 & 1 & 0 & 0\\ 0 & 0 & & & & & & & & \\ 0 & 0 & 0 & 0 & 0 & 0 & 0 & 0 & \cos\alpha_1 & -\sin\alpha_1\\ 0 & 0 & 0 & 0 & 0 & 0 & 0 & 0 & \sin\alpha_1 & \cos\alpha_1 \end{bmatrix}. \tag{4.5}$$

The Lagrangian given by Eq. 4.1 is invariant under this tangent lifted action. We can also show, as was done for the single beanie case, that the constraint one-forms are invariant under the cotangent lifted action, making G a symmetry group. We refrain from including this calculation, but can be verified following Eq. 3.7. The constraint distribution is

$$\begin{aligned}\mathcal{D}_q = \text{span}\{&-a_1\sin\theta_1\frac{\partial}{\partial x_1} + a_1\cos\theta_1\frac{\partial}{\partial y_1} + \frac{\partial}{\partial\theta_1}, \cos\theta_1\frac{\partial}{\partial x_1} + \sin\theta_1\frac{\partial}{\partial y_1}, \frac{\partial}{\partial\phi_1},\\ &- a_2\sin(\theta_1+\theta_2)\frac{\partial}{\partial x_1} + a_2\cos(\theta_1+\theta_2)\frac{\partial}{\partial y_1} + \frac{\partial}{\partial\theta_1} - a_2\sin(\theta_1+\theta_2)\frac{\partial}{\partial x_2}\\ &+ a_2\cos(\theta_1+\theta_2)\frac{\partial}{\partial y_2} + \frac{\partial}{\partial\theta_2}, \cos(\theta_1+\theta_2)\frac{\partial}{\partial x_1} + \sin(\theta_1+\theta_2)\frac{\partial}{\partial y_1}\\ &+ \cos(\theta_1+\theta_2)\frac{\partial}{\partial x_2} + \sin(\theta_1+\theta_2)\frac{\partial}{\partial y_2}, \frac{\partial}{\partial\phi_2}\}.\end{aligned} \tag{4.6}$$

The tangent space to the orbit of the group action Φ is

$$T_q\text{Orb}(q) = \text{span}\{\frac{\partial}{\partial x_1}, \frac{\partial}{\partial y_1}, \frac{\partial}{\partial\theta_1}, \frac{\partial}{\partial x_2}, \frac{\partial}{\partial y_2}, \frac{\partial}{\partial x_p}, \frac{\partial}{\partial y_p}\}. \tag{4.7}$$

We again seek a suitable set of vector fields which span the intersection of $\mathcal{D}_q$ and $T_q\text{Orb}(q)$. We choose

$$\begin{aligned}S_q = \text{span}\{&-a_1\sin\theta_1\frac{\partial}{\partial x_1} + a_1\cos\theta_1\frac{\partial}{\partial y_1} + \frac{\partial}{\partial\theta_1} + a_1\sin\theta_1\frac{\partial}{\partial x_2} - a_1\cos\theta_1\frac{\partial}{\partial y_2} + \frac{\partial}{\partial\theta_2},\\ &\cos\theta_1\frac{\partial}{\partial x_1} + \sin\theta_1\frac{\partial}{\partial y_1} - \cos\theta_1\frac{\partial}{\partial x_1} - \sin\theta_1\frac{\partial}{\partial y_1},\\ &- a_2\sin\theta_1\frac{\partial}{\partial x_2} + a_2\cos\theta_1\frac{\partial}{\partial y_2} + \frac{\partial}{\partial\theta_2}, \cos\theta_1\frac{\partial}{\partial x_2} + \sin\theta_1\frac{\partial}{\partial y_2},\\ &\cos\theta_1\frac{\partial}{\partial x_p} + \sin\theta_1\frac{\partial}{\partial y_p}, -\sin\theta_1\frac{\partial}{\partial x_p} + \cos\theta_1\frac{\partial}{\partial y_p}\}.\end{aligned} \tag{4.8}$$

The vector fields above generate the nonholonomic momenta corresponding to 1) longitudinal translational momentum of beanie 1, 2) rotational angular momentum of beanie 1 about the contact point of its wheel, 3) longitudinal translational momentum of beanie 2 in the body-fixed frame of beanie 1, 4) rotational angular momentum of beanie 2 about the contact point of its wheel in the body-fixed frame of beanie 1, 5) longitudinal translational momentum of the entire system in the body-fixed frame of beanie 1, and 6) momentum of the entire system orthogonal to the forward translational direction of beanie 1. Those momenta are given in terms of variables on TQ as

$$\begin{aligned}J_{LT,1} &= m_1(\dot{x}_1+\dot{x}_p)\cos\theta_1 + m_1(\dot{y}_1+\dot{y}_p)\sin\theta_1,\\ J_{RW,1} &= -m_1a_1(\dot{x}_1+\dot{x}_p)\sin\theta_1 + m_1a_1(\dot{y}_1+\dot{y}_p)\cos\theta_1 + (B_1+C_1)\dot{\theta}_1 + B_1\dot{\phi}_1,\\ J_{LT,2} &= m_2(\dot{x}_2+\dot{x}_1+\dot{x}_p)\cos\theta_1 + m_2(\dot{y}_2+\dot{y}_1+\dot{y}_p)\sin\theta_1,\\ J_{RW,2} &= -m_2a_2(\dot{x}_2+\dot{x}_1+\dot{x}_p)\sin\theta_1 + m_2a_2(\dot{y}_2+\dot{y}_1+\dot{y}_p)\cos\theta_1\\ &\quad + (B_2+C_2)(\dot{\theta}_1+\dot{\theta}_2) + B_2\dot{\phi}_2,\\ J_X &= m_1(\dot{x}_1+\dot{x}_p)\cos\theta_1 + m_1(\dot{y}_1+\dot{y}_p)\sin\theta_1 + m_2(\dot{x}_2+\dot{x}_1+\dot{x}_p)\cos\theta_1 + m_2(\dot{y}_2+\dot{y}_1+\dot{y}_p)\sin\theta_1\\ &\quad + M\dot{x}_p\cos\theta_1 + M\dot{y}_p\sin\theta_1,\\ J_Y &= -m_1(\dot{x}_1+\dot{x}_p)\sin\theta_1 + m_1(\dot{y}_1+\dot{y}_p)\cos\theta_1 - m_2(\dot{x}_2+\dot{x}_1+\dot{x}_p)\sin\theta_1 + m_2(\dot{y}_2+\dot{y}_1+\dot{y}_p)\cos\theta_1\\ &\quad - M\dot{x}_p\sin\theta_1 + M\dot{y}_p\cos\theta_1.\end{aligned} \tag{4.9}$$

We again compute the evolution equations as

$$\dot{J}^{nhc} = \frac{\partial L}{\partial \dot{q}^i}\left[\frac{d\xi}{dt}\right]_Q^i.$$

The resulting evolution equations, in coordinates on TQ, are given by

$$\begin{aligned}
\dot{J}_{LT,1} &= -m_1((\dot{x}_1 + \dot{x}_p)\sin\theta_1 + m_1(\dot{y}_1 + \dot{y}_p)\cos\theta_1)\dot{\theta}_1, \\
\dot{J}_{RW,1} &= \dot{\theta}_1((-(m_1+m_2)a_1(\dot{x}_1+\dot{x}_p) + m_2a_1\dot{x}_2)\cos\theta_1(-(m_1+m_2)a_1(\dot{y}_1+\dot{y}_p) \\
&\quad + m_2a_1\dot{y}_2)\sin\theta_1) \\
\dot{J}_{LT,2} &= m_2\dot{\theta}_1\left(\cos\theta_1\left(\dot{y}_1+\dot{y}_2+\dot{y}_p\right) - \sin\theta_1\left(\dot{x}_1+\dot{x}_2+\dot{x}_p\right)\right), \\
\dot{J}_{RW,2} &= a_2m_2\dot{\theta}_1\left(-\cos\theta_1\left(\dot{x}_1+\dot{x}_2+\dot{x}_p\right) - \sin\theta_1\left(\dot{y}_1+\dot{y}_2+\dot{y}_p\right)\right), \\
\dot{J}_X &= \dot{\theta}_1(\sin\theta_1((M+m_1+m_2)\dot{x}_p + (m_1+m_2)\dot{x}_1 + m_2\dot{x}_2) + \cos\theta_1((M+m_1+m_2)\dot{y}_p \\
&\quad + (m_1+m_2)\dot{y}_1 + m_2\dot{y}_2)), \\
\dot{J}_Y &= \dot{\theta}_1(-\cos\theta_1((M+m_1+m_2)\dot{x}_p + (m_1+m_2)\dot{x}_1 + m_2\dot{x}_2) - \sin\theta_1((M+m_1+m_2)\dot{y}_p \\
&\quad + (m_1+m_2)\dot{y}_1 + m_2\dot{y}_2)).
\end{aligned} \tag{4.10}$$

Eq. 4.9 can be solved to write Eq. 4.10 in terms of the components of nonholonomic momenta.

Stability. In Chapter 3 we proved that given an arbitrary initial rotor angle, i.e., initial spring deformation coupling the cart to the rotor, all of the Chaplygin beanie's angular momentum about the contact point at its wheel is converted into longitudinal translational momentum. More specifically, we showed that, for all trajectories corresponding to the level set $p_x^2 + p_y^2 = 0$, the longitudinal translational momentum of the agent asymptotically approaches a value that can be computed as a function of its initial rotor angle. We naturally ask a similar question when considering two Chaplygin beanies. Firstly, we wish to investigate the conversion of angular momentum to longitudinal translational momentum in the system.

4.2 Dynamic Entrainment

Consider the case of two Chaplygin beanies, equipped with linear torsional springs in the manner discussed previously, sitting atop a platform with translational compliance. Given arbitrary initial deformations in the rotor of each agent relative to its body, the asymptotic difference in the headings of the agents approaches a small number. This phenomena is called *dynamic entrainment* and is illustrated in Fig. 4.2. For this simulation, the initial heading of the blue agent was $\theta_1(0) = 0$, and $\theta_2(0) = \pi/3$ for the red agent. This entrainment of Chaplygin beanies on a translationally compliant platform has been shown in simulation to to maintain up until a particular value of the ratio $\frac{M_{platform}}{m_{beanie}}$ [2], where $M_{platform}$ and m_{beanie} are the total masses of the platform and Chaplygin beanie agent, respectively.

The value at which entrainment between two Chaplygin beanies fails is best visualized by figures showing the asymptotic heading of each beanie. Sweeping through a range of $\frac{M_{platform}}{m_{beanie}}$, we perform a simulation and from it extract the asymptotic heading of each agent. Plotting this on a log scale shows a bifurcation-like phenomenon, first illustrated in [2], but explored again here for thoroughness. Fig. 4.3 clarifies the asymptotic behavior of Chaplygin beanies effectively as a function of platform mass. As presented in [2], this is reminiscent of a bifurcation where the bifurcation, or control, parameter is $\frac{M_{platform}}{m_{beanie}}$. The reduced representation of the dynamics obtained from the evolution equations presented in the previous section will give greater insight into proving this bifurcation-like behavior.

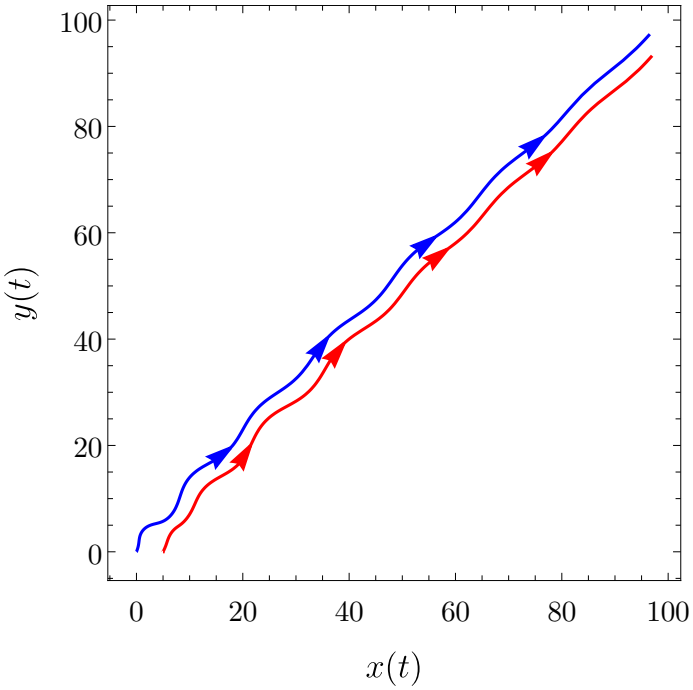

Figure 4.2: (x, y) trajectories of two Chaplygin beanies after given arbitrary initial rotor angles and different initial headings.

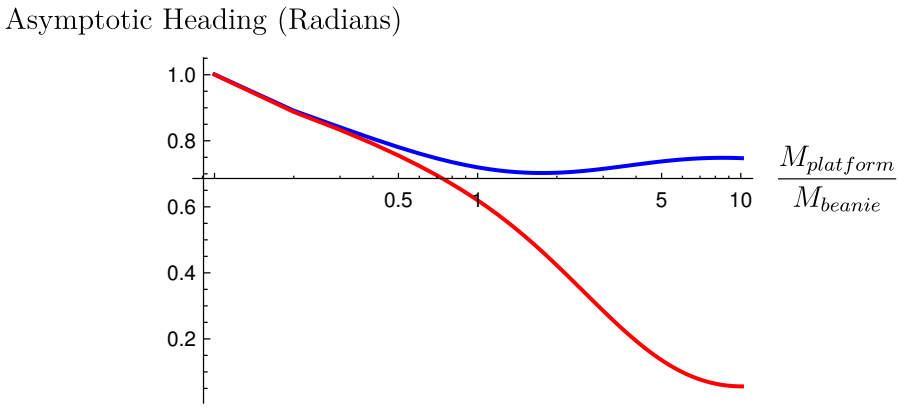

Figure 4.3: Asymptotic headings of two Chaplygin beanies as a function of the parameter $\frac{M_{platform}}{m_{beanie}}$.

Chapter 5

A Cylindrical-shaped Agent in an Inviscid Fluid with Point Vortices

We have so far introduced a multi-agent system for which the coupling between agents is encapsulated by a platform through which agents are constrained via nonholonomic constraints in the form of no-slip conditions on their wheels. While this model for an ambient medium provides a basis for studying interactions and coordination among agents, many real systems lack this direct model of coupling, necessitating the incorporation of elasticity or, in this case, fluid dynamics to more appropriately model coupling due to the medium. In this chapter, we introduce a dynamic model for a novel fluid-propulsive aquatic vehicle in an ideal fluid that exerts control over its motion using impulsive fluid-ejection events. The control input for the system is modeled as an instantaneous placement of a pair of symmetrically located counter-rotating point vortices. A snapshot of a simulation for this system after shedding some number of directed vortex pairs is shown in Fig. 5.1.

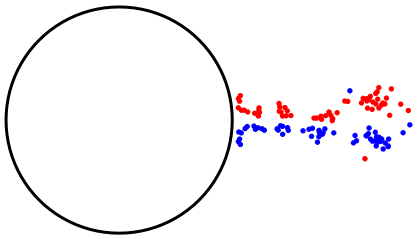

Figure 5.1: A planar body in an ideal fluid shedding directed vortex pairs to achieve locomotion.

The distilled nature of this system lends itself to various investigations into how solid bodies interact with vorticity in an inviscid fluid. This particular model also embodies the resulting behavior of aquatic organisms that can locomote via forcing fluid through a cavity in their body, e.g., jellyfish, squid, and salps.

5.1 Dynamic Model

The study of fluid-solid interactions in the plane has historically involved looking at the dynamics of such systems in the complex plane as well as conformal mapping techniques for generating interesting rigid body geometries [27], [41], [42]. Here we are interested in a simple conformal

map that results in scaling the unit disc, or circular cylinder, to a disc of radius R. Such a map takes coordinates in the preimage space, which we denote with coordinates ζ, to coordinates in the scaled coordinates, which we denote by z. Such a map takes the following form.

$$z(\zeta) = R\zeta \tag{5.1}$$

Since we are interested in the impulsive control of an aquatic vehicle taking on the geometry of a circular cylinder, we won't concern ourselves with the effects of different scaling values and let $R = 1$ in our simulations, making Eq. (5.1) the identity map.

5.1.1 Vortex Velocities and the Complex Potential

In understanding the vortex velocities relative to the cylinder, it is necessary to first write the complex potential for the system. Such a complex potential is the result of superposing the complex potential for a freely moving cylinder with the complex potential for each vortex in the flow.

$$w(z) = w_B(z) + \sum_{k=1}^{N} w_v^k(z) \tag{5.2}$$

Eq. (5.2) is the sum of the complex potential for a cylinder, $w_B(z)$, and the complex potential for each vortex, $w_v^k(z)$. The individual complex potentials are given below.

$$w_B = \xi_x R^2 z^{-1} + i\xi_y R^2 z^{-1} \tag{5.3}$$

$$w_v^k(z) = \Gamma_k i\big(\log(z - z_k) - \log(z - \frac{R^2}{\bar{z_k}}) + \log(z)\big) \tag{5.4}$$

This ensures that the circulation introduced by a vortex at z_k is nullified by the image vortices placed at $z = \frac{R^2}{\bar{\zeta_k}}$ and z with strengths corresponding to Eq. (5.4). The quantity $z = \frac{R^2}{\bar{z_k}}$ is recognized as a vortex at the image point with respect to the center of the circular cylinder. Let ξ_x, ξ_y, and ξ_θ be the linear and angular velocities of the cylinder in the body frame of the cylinder. The complex potential for a circular cylinder in the presence of N point vortices is then given by

$$w(z) = \xi_x w_1(z) + \xi_y w_2(z) + \sum_{k=1}^{N} \Gamma_k i\big(\log(z - z_k) - \log(z - \frac{R^2}{\bar{z_k}}) + \log(z)\big). \tag{5.5}$$

Note that the complex potential $w_1(z) = R^2 z^{-1}$ and $w_2(z) = R^2 z^{-1} i$. The complex potential for the kth vortex must exclude singular terms when computing its gradient, giving us

$$w_k(z) = w(z) - \Gamma_k i \log(z - z_k). \tag{5.6}$$

Finally, we can compute the velocity of each vortex with respect to the body frame of the cylinder by taking the gradient of the conjugate of Eq. (5.6) with respect to z [43].

$$\dot{z_k} = \big(\frac{d\bar{w}_k}{dz} - (\xi_x + i\xi_y)\big) \tag{5.7}$$

Since Eq. (5.7) is written with respect to the body frame of the cylinder, its real and imaginary parts will give the corresponding components in $\dot{\mathbf{q}}_v$ when added to the velocity of the cylinder in the inertial frame. Let $\dot{x}_k = \mathrm{Re}(\dot{z_k})$ and $\dot{y}_k = \mathrm{Im}(\dot{z_k})$.

5.1.2 Conservation of Total Momentum

We develop the components of Eq. (5.15) based on conservation of total momentum and express momentum terms for the vortices using the classical approach of complex potentials. We draw inspiration from [43], [32], and [27] in our understanding the momentum terms. Let $\mathbf{L}$ and $\mathbf{A}$ be the total linear and angular momentum of the system, respectively, and express them as

$$\mathbf{L} = c \begin{bmatrix} \xi_x \\ \xi_y \end{bmatrix} + \mathbf{P} \tag{5.8}$$

and

$$\mathbf{A} = \pi \mathbf{k}. \tag{5.9}$$

$\mathbf{P}$ and $\pi\mathbf{k}$ represent the linear and angular momentum contribution due to the point vortices in the flow and are computed as follows. The parameter c represents the cylinder mass plus the *added mass* of the cylinder, written as $c = m + \pi R^2$ where we assume the fluid to be of unit density. We let $\boldsymbol{\xi} = \begin{bmatrix} \xi_x & \xi_y & \xi_\theta \end{bmatrix}^\top$ be the linear and angular velocities of the cylinder in the body frame. If $z_k = x_k + iy_k$ is the location of the kth vortex, we can define the linear momentum contribution due to N point vortices to be

$$P = -\sum_{k=1}^{N} \frac{\Gamma_k}{2\pi R} \left(z_k - \frac{R^2}{\bar{z}_k} \right) i \tag{5.10}$$

and define $\mathbf{P} = \begin{bmatrix} \mathrm{Re}(P) & \mathrm{Im}(P) \end{bmatrix}^\top$. After extracting the real and imaginary parts of $\mathbf{P}$, we write

$$\mathbf{P} = \begin{bmatrix} \mathrm{Re}(P) \\ \mathrm{Im}(P) \end{bmatrix} = \begin{bmatrix} -\sum_{k=1}^{N} \frac{\Gamma_k}{2\pi} (-y_k + R^2 \frac{y_k}{x_k^2 + y_k^2}) \\ -\sum_{k=1}^{N} \frac{\Gamma_k}{2\pi} (x_k - R^2 \frac{x_k}{x_k^2 + y_k^2}) \end{bmatrix} \tag{5.11}$$

Eq. (5.11) is the final representation of the linear momentum due to N point vortices. We then write the angular momentum as

$$\pi = -\frac{1}{2} \sum_{k=1}^{N} \Gamma_k (x_k^2 + y_k^2). \tag{5.12}$$

We can finally write the conservation of total momentum and from it compute the velocity of the cylinder in the body frame. Let $M = \begin{bmatrix} c & 0 & 0 \\ 0 & c & 0 \\ 0 & 0 & I \end{bmatrix}$ be the mass matrix for the cylinder, where I is the rotational inertia of the cylinder.

$$\begin{bmatrix} \mathrm{Re}(P) \\ \mathrm{Im}(P) \\ \pi \end{bmatrix} + M \begin{bmatrix} \xi_x \\ \xi_y \\ \xi_\theta \end{bmatrix} = \begin{bmatrix} \mathrm{Re}(P_0) \\ \mathrm{Im}(P_0) \\ \pi_0 \end{bmatrix} \tag{5.13}$$

Quantities subscripted with a zero indicate the evaluation of that quantity at time $t = 0$. That is, the initial momentum of the system is on the right side of Eq. (5.13). Upon rearranging terms, the velocity of the cylinder in the body frame is expressed as

$$\boldsymbol{\xi} = \begin{bmatrix} \xi_x \\ \xi_y \\ \xi_\theta \end{bmatrix} = M^{-1} \left(\begin{bmatrix} \mathrm{Re}(P_0) \\ \mathrm{Im}(P_0) \\ \pi_0 \end{bmatrix} - \begin{bmatrix} \mathrm{Re}(P) \\ \mathrm{Im}(P) \\ \pi \end{bmatrix} \right). \tag{5.14}$$

Though our aquatic vehicle sheds directed vortex pairs to achieve locomotion, the underlying fluid-mechanical model is that of a circular cylinder in a flow of N point vortices. It is necessary to acknowledge, however, that the number of vortices is increasing at each instance of actuation. We let $\mathbf{q}_c = \begin{bmatrix} x_c & y_c & \theta_c \end{bmatrix}^\top \in SE(2)$ be the position and orientation of the cylinder with respect to the inertial frame and let $\mathbf{q}_v = \begin{bmatrix} x_c + x_1 & y_c + y_1 & \cdots & x_c + x_N & y_c + y_N \end{bmatrix}^\top$ be the positions of the vortices in the inertial frame, where each pair $(x_k, y_k) \in \mathbb{R}^2$ is written in the body frame of the cylinder. Since the number of vortices can be large, it is necessary that we establish a designation for circulation sign. Counter-clockwise rotating point vortices are colored red and assumed positive, and clockwise rotating point vortices are given the color blue and assumed negative. Given $\mathbf{q}_c$ and $\mathbf{q}_v$, we write $\mathbf{q} = \begin{bmatrix} \mathbf{q}_c & \dot{\mathbf{q}}_c & \mathbf{q}_v \end{bmatrix}^\top$ to represent the full state variables for the system given N point vortices in the flow. Thus, we seek a form for the continuous dynamics in the form

$$\dot{\mathbf{q}} = \begin{bmatrix} \dot{\mathbf{q}}_c \\ \ddot{\mathbf{q}}_c \\ \dot{\mathbf{q}}_v \end{bmatrix} = f(\mathbf{q}, \dot{\mathbf{q}}). \tag{5.15}$$

5.1.3 Cylinder Dynamics in the Inertial Frame

Eq. (5.14) is the velocity of the cylinder in the body frame. To obtain the velocity of the cylinder with respect to the inertial frame, we apply the rotation matrix

$$\mathbf{R} = \begin{bmatrix} \cos(\theta_c) & -\sin(\theta_c) & 0 \\ \sin(\theta_c) & \cos(\theta_c) & 0 \\ 0 & 0 & 1 \end{bmatrix}. \tag{5.16}$$

This gives us $\dot{\mathbf{q}}_c$ from Eq. (5.15) and can be written as

$$\dot{\mathbf{q}}_c = \mathbf{R}^\top \boldsymbol{\xi}. \tag{5.17}$$

The velocity of each vortex can be written as

$$\dot{\mathbf{q}}_v = \begin{bmatrix} \dot{x}_c + \dot{x}_k \\ \dot{y}_c + \dot{y}_k \end{bmatrix}. \tag{5.18}$$

For every $k \in 1, ..., N$. Note that the velocity of each vortex is a function of the spatial derivative of its complex potential, requiring us to recompute Eqs. (5.5), (5.6), and (5.7) at each vortex shedding event. Given Eq. (5.17) and Eq. (5.18), all that is left to compute is the acceleration of the cylinder. Such a task equates to simply taking time derivatives of $\dot{\mathbf{q}}_c$. There are some subtleties to this, primarily in the calculation of initial accelerations. The acceleration of the cylinder in the body frame can be obtained by computing $\frac{d}{dt}\boldsymbol{\xi}$, but to obtain the acceleration in the inertial frame, we must use the following identity.

$$\frac{d\boldsymbol{\xi}}{dt} = \mathbf{R}\ddot{\mathbf{q}}_c + \dot{\mathbf{R}}\dot{\mathbf{q}}_c = \mathbf{R}\ddot{\mathbf{q}}_c + \mathbf{R}(\xi_\theta \mathbf{k} \times \dot{\mathbf{q}}_c) \tag{5.19}$$

So we need only compute one term in Eq. (5.19), $\dot{\boldsymbol{\xi}}$, and the rest is obtained from derivatives already computed. The relevant terms in $\boldsymbol{\xi}$ for which we must take time derivatives are $\mathbf{P}$ and π. These are given in Eqs. (5.20), (5.21), and (5.22).

$$\begin{aligned} \frac{d}{dt}\operatorname{Re}(P) = -\sum_{k=1}^{N} \frac{\Gamma_k}{2\pi}\big(&- \dot{y}_k + R^2(\dot{y}_k(2x_k\dot{x}_k + 2y_k\dot{y}_k)\times \\ &(x_k^2 + y_k^2)^{-2} + \dot{y}_k y_k (x_k^2 + y_k^2))\big) \end{aligned} \tag{5.20}$$

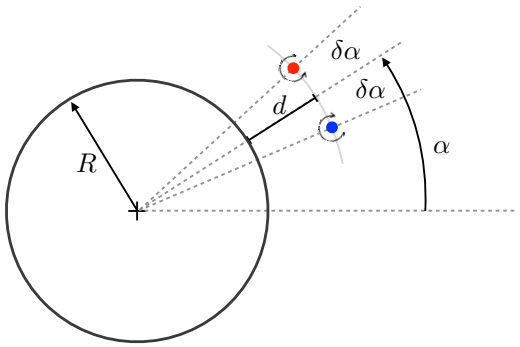

Figure 5.2: Diagram illustrating the ejection mechanism for the aquatic vehicle

$$\frac{d}{dt}\operatorname{Im}(P) = -\sum_{k=1}^{N}\frac{\Gamma_k}{2\pi}\big(\dot{x}_k - R^2(\dot{x}_k(2x_k\dot{x}_k + 2y_k\dot{y}_k)\times (x_k^2+y_k^2)^{-2} + \dot{x}_k y_k(x_k^2+y_k^2))\big) \tag{5.21}$$

$$\frac{d}{dt}\pi = -\frac{1}{2}\sum_{k=1}^{N}\Gamma_k(2x_k\dot{x}_k + 2y_k\dot{y}_k) \tag{5.22}$$

This allows us to fully compute $\dot{\boldsymbol{\xi}}$, recognizing the presence of the vector representing the initial acceleration of the cylinder.

$$\dot{\boldsymbol{\xi}} = M^{-1}\left(\begin{bmatrix}\dot{\mathbf{P}}_0\\ \dot{\pi}_0\end{bmatrix} - \begin{bmatrix}\dot{\mathbf{P}}\\ \dot{\pi}\end{bmatrix}\right) \tag{5.23}$$

With all of the relevant terms for $\dot{\boldsymbol{\xi}}$ computed, we can compute $\ddot{\mathbf{q}}_c$, Eq. (5.19), finalizing the continuous dynamics of Eq. (5.15).

5.1.4 Impulsive Control Formulation

Given the dynamics for the aquatic vehicle, we can now define what it means to impulsively control it. The continuous dynamics can also be seen as the *drift* dynamics for the system. That is, under no control input, the dynamics obey Eq. (5.15). We wish to clarify the control input as well as write down the full version of the dynamics given discrete-time inputs to the system. Fig. 5.2 provides a visualization for the actuation mechanism. This can be interpreted as the aquatic vehicle ejecting pairs of point vortices at any angle α around its boundary. This kind of system is often described as a *hybrid* system, containing both continuous as well as impulsive dynamics. Eq. (5.24) and (5.25) give a general description of the system [44].

$$\ddot{\mathbf{q}} = f(\mathbf{q}, \dot{\mathbf{q}}), \qquad t \neq t_j \tag{5.24}$$

$$\mathbf{q}(t_j^+) = \mathbf{C}_j\mathbf{q}(t_j^-) + \mathbf{D}_j\mathbf{v}_j, \qquad \begin{matrix} t = t_j \\ \forall j \in 1, ..., J \end{matrix} \tag{5.25}$$

The notation $()^-$ and $()^+$ denote the time before and after the impulsive control input $\mathbf{v}_j$ is applied, respectively. Matrices $\mathbf{C}_j$ and $\mathbf{D}_j$ ensure that only the state variables affected at time $t = t_j$ by the impulse are updated, making them diagonal matrices, the entries for which are either 0, if the state variable remains unaffected, or 1, if the state variable is to be updated due to the impulse.

Before proceeding to the definition of $\mathbf{v}_j$, we note that Eq. (5.24) and Eq. (5.25) can be reduced in that the vortex state variables are not impacted by $\mathbf{v}_j$, allowing us to consider only the impact on the cylinder velocities. We leave the continuous dynamics unchanged, but rewrite the impulsive part of the dynamics so as to only contain the cylinder velocities.

$$\dot{\mathbf{q}}_c(t_j^+) = \mathbf{C}_j\dot{\mathbf{q}}_c(t_j^-) + \mathbf{D}_j\mathbf{v}_j, \qquad t = t_j \tag{5.26}$$

Since all of $\dot{\mathbf{q}}_c$ is impacted at the time of impulse, let $\mathbf{C}_j$ be the 3×3 identity matrix and let $\mathbf{D}_j$ be $\mathbf{R}M^{-1}$. $\mathbf{v}_j$ will ultimately be an addition of momentum to the system, so we must premultiply by the inverse of the mass matrix to obtain a velocity update in the inertial frame. Eq. (5.26) can then be written as

$$\dot{\mathbf{q}}_c(t_j^+) = \dot{\mathbf{q}}_c(t_j^-) + \mathbf{R}M^{-1}\mathbf{v}_j, \qquad t = t_j.$$

In this work the time between ejection events, $\Delta t_{j+1,j} = t_{j+1} - t_j$, is constant. That is, we do not choose *when*, but at what strength, to eject a vortex pair. We leave the optimization of time of impulse for this system to future work. We can now define the impulse $\mathbf{v}_j$. Before doing so, we make note of the fact that at each discrete ejection event, the dimension of the vector in Eq. (5.15) increases by two.

Impulsive Control Input. In this section we describe the impulse to the system, $\mathbf{v}_j$. Given our description of the geometry in Fig. 5.2, we write the momentum contribution due to placing two point vortices into the flow with opposite circulations as

$$\mathbf{v}_j = \begin{bmatrix} \frac{\Gamma_j}{2\pi}\big((R+d) + \frac{R^2}{R+d}\big)\big(\sin(\alpha - \delta\alpha) - \sin(\alpha + \delta\alpha)\big) \\ \frac{\Gamma_j}{2\pi}\big((R+d) + \frac{R^2}{R+d}\big)\big(\cos(\alpha + \delta\alpha) - \cos(\alpha - \delta\alpha)\big) \\ \frac{1}{2}\Gamma_j(R+d)^2\big(\cos^2(\alpha - \delta\alpha) - \cos^2(\alpha + \delta\alpha) + \sin^2(\alpha + \delta\alpha) - \sin^2(\alpha - \delta\alpha)\big) \end{bmatrix}. \tag{5.27}$$

The vector $\mathbf{v}_j$ is just the momentum of the ejected vortices in the body frame. $\mathbf{R}M^{-1}$ casts it into the inertial frame while dividing by the mass and inertial components of the mass matrix. Our definition of Eq. (5.27) allows us to interpret Eq. (5.1.4) in the following way. At time $t = t_j$, a pair of vortices is ejected with momenta corresponding to $\mathbf{v}_j$. Due to this discrete event of adding momentum to the fluid, the velocity of the cylinder must be adjusted to obey conservation of momentum.

5.2 Dynamic Entrainment

We have fully developed the dynamic model for a cylinder capable of impulsively ejecting directed vortex pairs in an inviscid fluid. In this section, we shift our perspective from impulsive control and first analyze the behavior of a stationary cylinder as it is impacted by directed vortex pairs originating from an imaginary neighboring agent. Our dynamic model comprises only a single agent impacted by vortices placed in the flow. The dynamics of multiple cylinders capable of shedding directed vortex pairs demands tools from conformal mapping theory in multiply-connected domains and is currently work in progress. The hope is for our analysis to give insight into what constitutes a mutually beneficial behavior for a system comprising two such cylindrical-shaped agents.

5.2.1 Entrainment and Impact Angle

As an initial step toward understanding the dynamics of a cylindrical-shaped agent as it is impacted by the incoming flow induced by a neighboring agent, we place directed vortex pairs in the flow at various ejection angles and characterize the resulting trajectory of the cylinder. We investigate the result of impact at ejection angles by specifying an incrementally larger α as shown in Fig. 5.2. The ejection angles we will analyze are 0, $\frac{\pi}{30}$, $\frac{\pi}{25}$, and $\frac{\pi}{20}$. We designate $\delta\alpha = 0.1$ radians and $d = 0.1$ for each analysis.

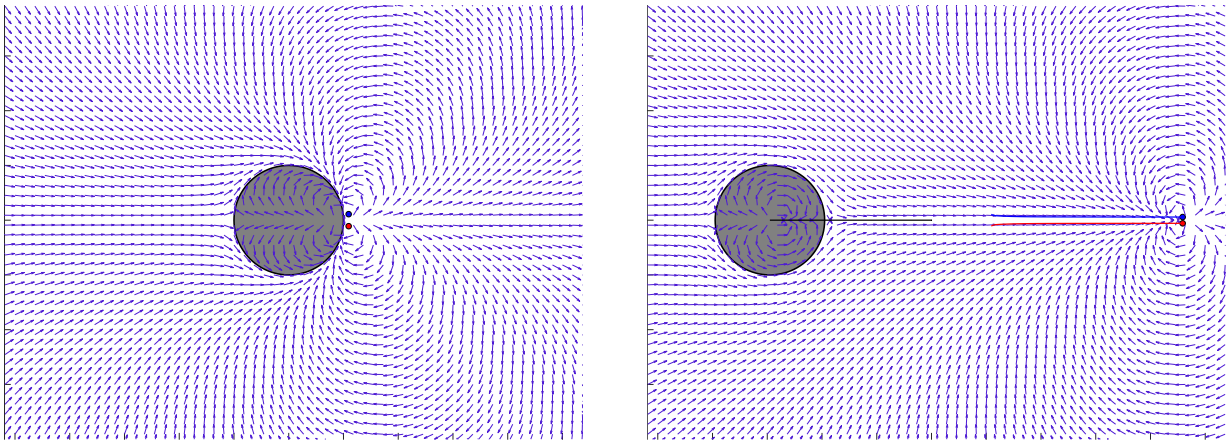

(a) A simulation snapshot of a cylindrical-shaped agent ejecting vortices at $t = t_0$ with an ejection angle of $\alpha = 0$.

(b) A simulation snapshot of a cylindrical-shaped agent ejecting vortices at $t = t_f$ with an ejection angle of $\alpha = 0$.

Figure 5.3: Two snapshots of a simulation for an ejection angle of $\alpha = 0$.

Fig. 5.3 shows a cylinder ejecting a pair of counter-rotating point vortices at an ejection angle of $\alpha = 0$. The flow field is visualized by blue vectors normalized in length to ensure a clear understanding of flow direction. These vectors actually decrease in magnitude as the distance from flow sources increases. Imagine now a *second* cylindrical-shaped agent to the right of the one shown above ejecting a pair of vortices. We can gain an understanding of the second agent's approximate behavior by viewing the dynamics corresponding to impact of the vortex pair as they flow from their final position in Fig. 5.3 to the second agent.

This initial experiment already exhibits interesting behavior. Fig. 5.4 shows that given an impact angle of $\alpha = 0$, the pair of counter-rotating point vortices adhere to the surface of the agent and roll around its body until shedding off the opposite side of the cylinder. In their doing so, the vortices have effectively pulled the cylinder to the left by some visibly nonzero distance. This is clearly seen in Fig. 5.5. Note that the green circle indicates the initial position of the cylinder and the red circle indicates its final position.

The extent to how such impacts by directed vortex shedding can aid in the locomotion of a neighboring agent is what we seek to elucidate. In particular, we can not only induce significant linear motion as shown in Fig. 5.4, but can also induce the cylinder to move in both the X and Y directions by shedding a directed vortex pair at various angles toward the second cylinder. We refrain from including images of the ejecting cylinder as its forward motion is maintained, but altered only by the angle at which it sheds a directed vortex pair. Fig. 5.6 shows the trajectories resulting from impact angles of $\frac{\pi}{30}$, $\frac{\pi}{25}$, and $\frac{\pi}{20}$.

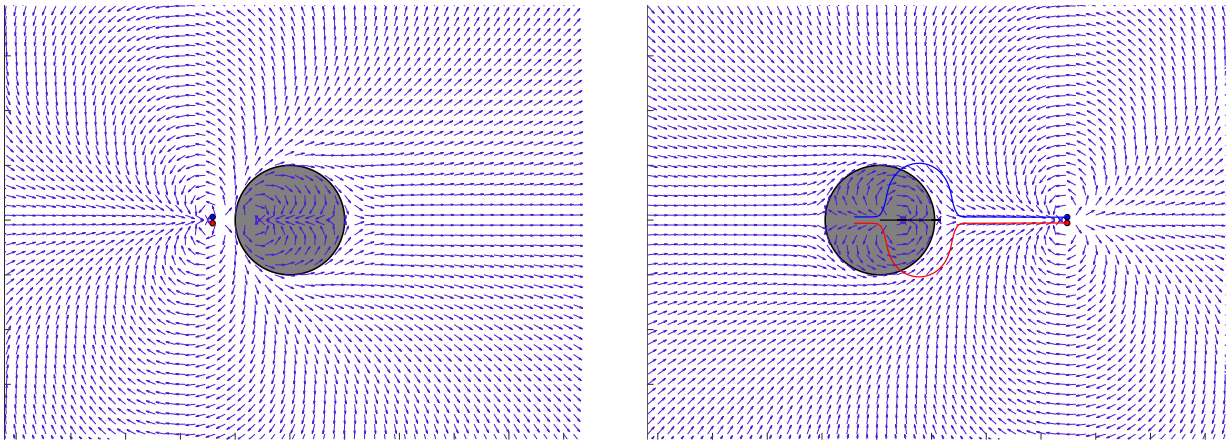

(a) A simulation snapshot of a cylindrical-shaped agent being impacted by a pair of point vortices corresponding to an impact angle of $\alpha = 0$.

(b) A simulation snapshot of a cylindrical-shaped agent being impacted by a pair of point vortices corresponding to an impact angle of $\alpha = 0$.

Figure 5.4: Two snapshots of a simulation of a cylinder being impacted by vortices at an impact angle of $\alpha = 0$.

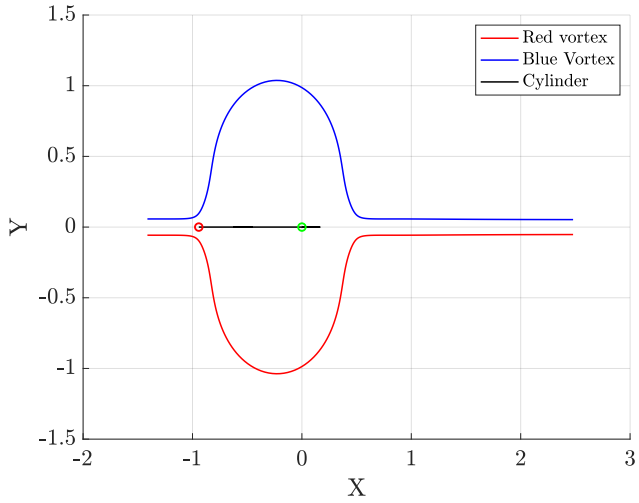

Figure 5.5: Trajectories in the world frame corresponding to the impact illustrated in Fig. 5.4.

5.3 Position Stabilization via Vortex Strength Control

We wish to choose a setpoint in the plane and impulsively eject pairs of vortices to stabilize about that point. The means of actuation for the aquatic vehicle is described as ejecting fluid through a cavity which generates the two-dimensional cross-section of a vortex ring, which we model simply as placing counter-rotating vortex pairs into the flow. Such an actuator was studied at some length in [45] and [46] for use in bioinspired thrusters for underwater robots. It is natural to assume control over the strength of the vortex pair depicted in Fig. 5.2, meaning we directly control how large the impulse is as a time-parameterized function of Γ_j. Rather than assume control over α as well, we simply assume α to be the angle such that the ejection event always pulls, or pushes, the system toward, or away from, the setpoint.

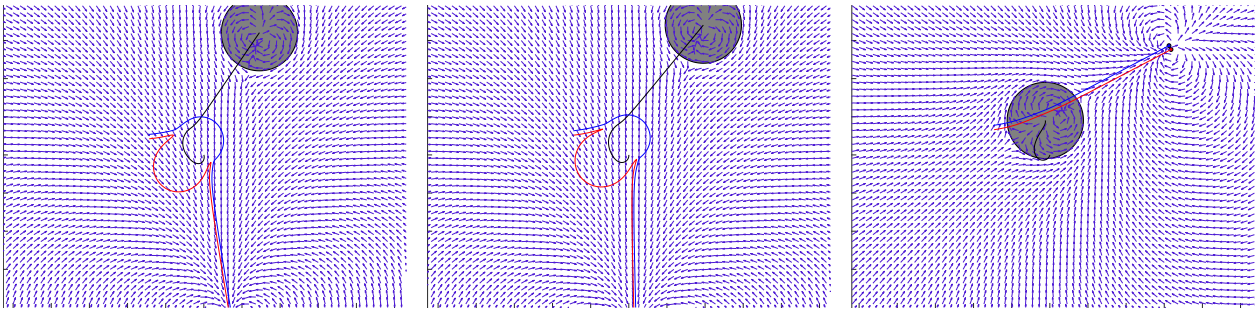

Figure 5.6: From left to right: trajectories resulting from impact angles of $\frac{\pi}{30}$, $\frac{\pi}{25}$, and $\frac{\pi}{20}$

5.3.1 PD Control Law on Vortex Strength

Controlling the strength of the vortex pair at each ejection event is accomplished using a standard proportional-derivative control law. Given a setpoint (x_d, y_d), we close the feedback loop on the measured variables (x_c, y_c) and define the error to be

$$\begin{aligned} e(t) =& \sqrt{e_x(t)^2 + e_y(t)^2} \\ =& \sqrt{(x_d - x_c)^2 + (y_d - y_c)^2} \end{aligned} \tag{5.28}$$

and let $\Gamma_j(t)$ be equal to the following function.

$$\Gamma_j(t) = K_p e(t) + K_d \frac{d}{dt} e(t) + K_i \int_0^t e(t)dt \tag{5.29}$$

Using the proposed control law, we let $x_d = 1, y_d = 1$ to verify its ability to stabilize about the desired setpoint with $K_p = 0.25$, $K_d = 1.15$, and $K_i = 0$. Fig. 5.7 shows the trajectory of the cylinder with initial conditions $\mathbf{q} = \mathbf{0}$ with no initial vortices in the flow. We can see from

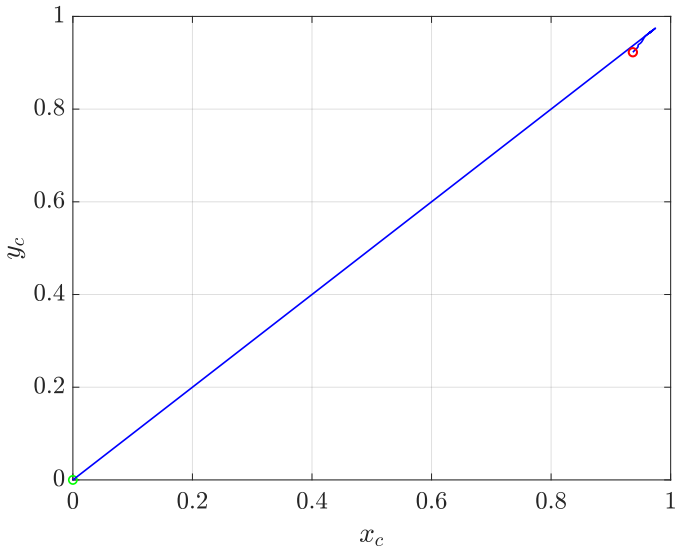

Figure 5.7: Trajectory of cylinder under a PD control law stabilizing about point $x_d = 1, y_d = 1$ with initial conditions $\mathbf{q}_0 = \mathbf{0}$

Figure 5.7 that the system stabilizes within some basin of attraction of the setpoint under the PD control law. Figure 5.8 shows that the velocity of the cylinder approaches zero as the system

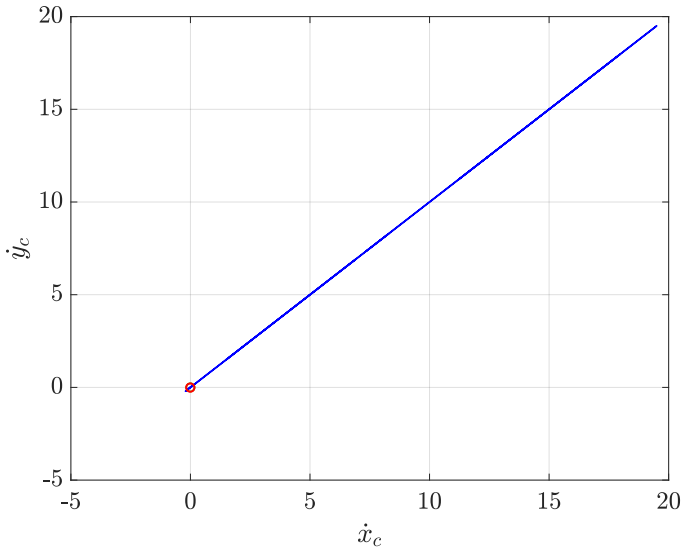

Figure 5.8: Inertial velocity of the cylinder while controlling to $x_d = 1, y_d = 1$ with initial conditions $\mathbf{q}_0 = \mathbf{0}$

approaches the setpoint. Fig. 5.8 depicts the initial velocity of the cylinder (green circle) and its final velocity (red circle). The green circle is hardly visible as the final velocity of the cylinder is close to zero, overlapping the green circle denoting the initial velocity. Fig. 5.7 clearly shows undershoot, indicating further tuning of the PID controller would be necessary to close the gap on this error. However, this example demonstrates the extent to which a PID controller can be used with a highly nonlinear system for which the state space grows at each vortex shedding event.

Chapter 6

Conclusions and Future Work

We presented three dynamical systems for which agents are coupled by the dynamics of an ambient medium. The first of these illustrates the utility of nonholonomic reduction for such systems. We developed the reduced equations for a single Chaplygin beanie on a movable platform and proved that, given a nonzero initial deformation in the spring coupling the vehicle's rotor to its body, the dynamics are asymptotically stable, with all of the system's angular momentum being converted into forward translational momentum. We then characterized motion primitives for the same system when we assume actuation of the platform and demonstrated that it is possible to station-keep and scatter passive Chaplygin beanies. The second of these systems then illustrated the extent to which agents can be *directly* coupled through an ambient medium by placing two Chaplygin beanies on a movable platform. Using nonholonomic reduction, we laid the groundwork for proving mainly two things: 1) that both beanies will asymptotically locomote away stably, regardless of their initial heading or initial rotor angle, and 2) the entrainment of two Chaplygin beanies, that is, the asymptotic difference in the headings of two beanies approaches a small number less than or equal to $\pi/20$, independent of initial heading or rotor angle. The third of these systems graduated from an environment that directly couples the locomotion of agents and introduced a cylindrical-shaped aquatic agent capable of shedding directed vortex pairs discretely in time. A distinct feature of this dynamical system is its inevitable growth in the dimension of the state space, a complexity not seen in many dynamical systems. We first reformulated the dynamics of a circular cylinder in the presence of point vortices in a way clarifying its impulsive way of shedding vortices. We then demonstrated that, in the presence of oncoming vortex shedding structures, a cylinder can be pulled toward or away from the direction in which the vortex pair was shed, effectively another example of entrainment in a system interacting with an ambient medium. Finally, we presented preliminary results for a position-stabilizing contoller on vortex strength, demonstrating its effectiveness on a highly nonlinear system for which the dimension of the state space grows at each vortex shedding event.

The single Chaplygin beanie on a platform can be further explored to classify various behaviors as they change as a function of parameters. Another problem that warrants exploration is an investigation into the behavior of a Chaplygin beanie when the model for this dynamical system is modified by restricting the motion of the platform to respond elastically, for example via a linear spring coupling the platform to the world frame. The two proofs stated above are open problems for this work and are currently being investigated by the author. With access to a reduced representation of the dynamics, solutions to these two problems will be much more approachable. In this thesis we modeled a *single* cylindrical-shaped agent capable of vortex shedding. Recent tools by Crowdy [47, 48, 49] have made it possible to begin modeling *multiple*

such agents through use of conformal mapping techniques in multiply-connected domains. Therefore, developing a model for multiple cylindrical-shaped agents capable of shedding vortices in an inviscid flow would advance the studies of multi-agent interactions through ambient media.

References

[1] S. Chaplygin. On the theory of motion of nonholonomic systems. the reducing-multiplier theorem. *Regular and Chaotic Dynamics*, 13:369–376, 08 2008.

[2] Scott Kelly, Rodrigo Abrajan-Guerrero, Jaskaran Grover, Matthew Travers, and Howie Choset. Planar Motion Control, Coordination and Dynamic Entrainment in Chaplygin Beanies. In *ASME 2018 Dynamic Systems and Control Conference*. American Society of Mechanical Engineers Digital Collection, 2018.

[3] Jerrold E. Marsden, Richard Montgomery, and Tudor S. RaÈiu. *Reduction, Symmetry, and Phases in Mechanics*, volume 436. American Mathematical Society, 1990.

[4] Jerrold E. Marsden and Jürgen Scheurle. The reduced euler-lagrange equations. *Fields Institute Comm*, 1:139–164, 1993.

[5] Jerrold E. Marsden and Tudor Ratiu. *Introduction to Mechanics and Symmetry: A Basic Exposition of Classical Mechanical Systems*, volume 17. Springer Science & Business Media, 2013.

[6] Anthony M. Bloch, P. S. Krishnaprasad, Jerrold E. Marsden, and Richard M. Murray. Nonholonomic mechanical systems with symmetry. *Archive for Rational Mechanics and Analysis*, 136(1):21–99, 1996.

[7] S. David Kelly, M. J. Fairchild, P. M. Hassing, and P. Tallapragada. Proportional heading control for planar navigation: The Chaplygin beanie and fishlike robotic swimming. In *2012 American Control Conference (ACC)*, pages 4885–4890, June 2012.

[8] Anthony M Bloch, P S Krishnaprasad, Jerrold E Marsden, and Richard M Murray. Nonholonomic mechanical systems with symmetry. *Archive for Rational Mechanics and Analysis*, 136(1):21–99, dec 1996.

[9] Elie Shammas and Maurício de Oliveira. Motion planning for the snakeboard. *The International Journal of Robotics Research*, 31(7):872–885, 2012.

[10] T. Dear, S.D. Kelly, M. Travers, and H. Choset. Mechanics and control of a terrestrial vehicle exploiting a nonholonomic constraint for fishlike locomotion. In *Proceedings of ASME Dynamic Systems and Control Conference (DSCC)*, October 2013.

[11] T. Dear, S. D. Kelly, M. Travers, and H. Choset. Locomotive analysis of a single-input three-link snake robot. In *2016 IEEE 55th Conference on Decision and Control (CDC)*, pages 7542–7547, 2016.

[12] Tony Dear, Blake Buchanan, Rodrigo Abrajan-Guerrero, Scott David Kelly, Matthew Travers, and Howie Choset. Locomotion of a multi-link non-holonomic snake robot with passive joints. *The International Journal of Robotics Research*, 0(0):0278364919898503, 0.

[13] Vitaliy Fedonyuk and Phanindra Tallapragada. The Dynamics of a Chaplygin Sleigh with an Elastic Internal Rotor. *Regular and Chaotic Dynamics*, 24(1):114–126, 2019.

[14] David Nelson Beal, Franz S. Hover, Michael S. Triantafyllou, James C. Liao, and George V. Lauder. Passive propulsion in vortex wakes. 2006.

[15] Nicholas C Darnton, Linda Turner, Svetlana Rojevsky, and Howard C Berg. Dynamics of Bacterial Swarming. *Biophysical Journal*, 98(10):2082–2090, 2010.

[16] C M Lo, H B Wang, M Dembo, and Y L Wang. Cell movement is guided by the rigidity of the substrate. *Biophysical journal*, 79(1):144–152, jul 2000.

[17] Rodrigo Abrajan-Guerrero and Scott David Kelly. Elastic compliance versus joint actuation in an articulated swimming robot. *IFAC-PapersOnLine*, 51(13):167 – 173, 2018. 2nd IFAC Conference on Modelling, Identification and Control of Nonlinear Systems MICNON 2018.

[18] Tony Dear, Scott David Kelly, Matthew Travers, and Howie Choset. Mechanics and control of a terrestrial vehicle exploiting a nonholonomic constraint for fishlike locomotion. In *ASME 2013 Dynamic Systems and Control Conference*, pages V002T33A004–V002T33A004. American Society of Mechanical Engineers, 2013.

[19] Scott David Kelly and Rodrigo Abrajan-Guerrero. Propulsive heading control and damping-induced heading recovery for a free hydrofoil with an internal rotor.

[20] Tony Dear, Scott David Kelly, Matthew Travers, and Howie Choset. Dissipation-induced self-recovery in systems on principal bundles. In *ASME 2014 Dynamic Systems and Control Conference*, pages V001T11A004–V001T11A004. American Society of Mechanical Engineers, 2014.

[21] Matthew Travers, Julian Whitman, and Howie Choset. Shape-based coordination in locomotion control. *The International Journal of Robotics Research*, 37(10):1253–1268, 2018.

[22] Chaohui Gong, Daniel Goldman, and Howie Choset. Simplifying gait design via shape basis optimization. 06 2016.

[23] Rodrigo Abrajan-Guerrero, Jeff D. Eldredge, Stuart T. Smith, and Scott David Kelly. Quasisteady particle transport in slowly varying periodic streaming flows. *IFAC Proceedings Volumes*, 47(3):5859 – 5865, 2014. 19th IFAC World Congress.

[24] Ido Nitsan, Stavit Drori, Yair E Lewis, Shlomi Cohen, and Shelly Tzlil. Mechanical communication in cardiac cell synchronized beating. *Nature Physics*, 12(5):472–477, 2016.

[25] Tony Dear. *Extensions of the Principal Fiber Bundle Model for Locomoting Robots*. PhD thesis, Carnegie Mellon University, 2018.

[26] E Kanso, J E Marsden, C W Rowley, and J B Melli-Huber. Locomotion of Articulated Bodies in a Perfect Fluid. *Journal of Nonlinear Science*, 15(4):255–289, 2005.

[27] Hailong Xiong. *Geometric Mechanics, Ideal Hydrodynamics, and the Locomotion of Planar Shape -Changing Aquatic Vehicles*. PhD thesis, University of Illinois at Urbana-Champaign, 2007.

[28] S. D. Kelly and H. Xiong. Self-propulsion of a free hydrofoil with localized discrete vortex shedding: Analytical modeling and simulation. *Theoretical and Computational Fluid Dynamics*, 24(1):45–50, 2010.

[29] Scott David Kelly and Parthesh Pujari. Propulsive energy harvesting by a fishlike vehicle in a vortex flow: Computational modeling and control. *49th IEEE Conference on Decision and Control (CDC)*, pages 1058–1064, 2010.

[30] G Kirchhoff. *Vorlesungen über mathematische Physik: Mechanik*. Nineteenth Century Collections Online (NCCO): Science, Technology, and Medicine: 1780-1925. B.G. Teubner, 1876.

[31] Francis Alexander Tarleton. On a Problem in Vortex Motion. *Proceedings of the Royal Irish Academy (1889-1901)*, 2:617–619, 1891.

[32] Banavara N Shashikanth, Jerrold E Marsden, Joel W Burdick, and Scott D Kelly. The Hamiltonian structure of a two-dimensional rigid circular cylinder interacting dynamically with N point vortices. *Physics of Fluids*, 14(3):1214–1227, 2002.

[33] Bartosz Protas. Linear feedback stabilization of laminar vortex shedding based on a point vortex model. *Physics of Fluids*, 16(12):4473–4488, 2004.

[34] A V. Borisov, Ivan Mamaev, and S M. Ramodanov. Motion of a circular cylinder and n point vortices in a perfect fluid. *Regular and Chaotic Dynamics*, 8, 2005.

[35] Zhanhua Ma and B N Shashikanth. Dynamics and control of the system of a 2-D rigid circular cylinder and point vortices. *2006 American Control Conference*, pages 6 pp.–, 2006.

[36] Hassan Aref. Point vortex dynamics: A classical mathematics playground. *Journal of Mathematical Physics*, 48(6):65401, 2007.

[37] Joris Vankerschaver, Eva Kanso, and Jerrold E. Marsden. The Geometry and Dynamics of Interacting Rigid Bodies and Point Vortices. *The Journal of Geometric Mechanics*, 1, 2008.

[38] J. E. Marsden and T. S. Ratiu. *Introduction to Mechanics and Symmetry*. Springer-Verlag, 2nd edition, 1999.

[39] Emmy Noether and M. A. Tavel. Invariant variation problems. 1971.

[40] Scott Kelly. Entrainment and multiscale dynamics in vibrationally driven nonholonomic systems. *24th International Congress of Theoretical and Applied Mechanics*, 2016.

[41] Jennie Cochran, Eva Kanso, Scott David Kelly, Hailong Xiong, and Miroslav Krstić. Source Seeking for Two Nonholonomic Models of Fish Locomotion. *IEEE Transactions on Robotics*, 25:1166–1176, 2009.

[42] P. Tallapragada and S. D. Kelly. Reduced-order modeling of propulsive vortex shedding from a free pitching hydrofoil with an internal rotor. In *2013 American Control Conference*, pages 615–620, June 2013.

[43] L. M. Milne-Thomson. *Theoretical hydrodynamics*. Mamillan Pr., 1979.

[44] L A Sobiesiak and C J Damaren. Linear quadratic optimal control for systems with continuous and impulsive inputs. In *53rd IEEE Conference on Decision and Control*, pages 5071–5076, dec 2014.

[45] M. Krieg and K. Mohseni. Thrust characterization of a bioinspired vortex ring thruster for locomotion of underwater robots. *IEEE Journal of Oceanic Engineering*, 33(2):123–132, April 2008.

[46] Mike Krieg, Peter Klein, Robert Hodgkinson, and Kamran Mohseni. A Hybrid Class Underwater Vehicle: Bioinspired Propulsion, Embedded System, and Acoustic Communication and Localization System. *Marine Technology Society Journal*, 45:153–164, 2011.

[47] Darren Crowdy. A new calculus for two-dimensional vortex dynamics. *Theoretical and Computational Fluid Dynamics*, 24(1):9–24, Mar 2010.

[48] D. G. Crowdy, E. H. Kropf, C. C. Green, and M. M. S. Nasser. The Schottky–Klein prime function: a theoretical and computational tool for applications. *IMA Journal of Applied Mathematics*, 81(3):589–628, 06 2016.

[49] Darren Crowdy. *Solving Problems in Multiply Connected Domains*. Society for Industrial and Applied Mathematics, 2020.